

Stochasticity in materials structure, properties, and processing—A review

Robert Hull,¹ Paweł Kebinski,¹ Dan Lewis,¹ Antoinette Maniatty,² Vincent Meunier,³ Assad A. Oberai,² Catalin R. Picu,² Johnson Samuel,² Mark S. Shephard,² Minoru Tomozawa,¹ Deepak Vashishth,⁴ and Shengbai Zhang³

¹Department of Materials Science and Engineering & Center for Materials, Devices and Integrated Systems, Rensselaer Polytechnic Institute, Troy, New York 12180, USA

²Department of Mechanical, Aeronautical and Nuclear Engineering & Center for Materials, Devices and Integrated Systems, Rensselaer Polytechnic Institute, Troy, New York 12180, USA

³Department of Physics, Applied Physics, and Astronomy & Center for Materials, Devices and Integrated Systems, Rensselaer Polytechnic Institute, Troy, New York 12180, USA

⁴Department of Biomedical Engineering & Center for Materials, Devices and Integrated Systems, Rensselaer Polytechnic Institute, Troy, New York 12180, USA

(Received 28 July 2017; accepted 19 January 2018; published online 7 March 2018)

We review the concept of stochasticity—i.e., unpredictable or uncontrolled fluctuations in structure, chemistry, or kinetic processes—in materials. We first define six broad classes of stochasticity: equilibrium (thermodynamic) fluctuations; structural/compositional fluctuations; kinetic fluctuations; frustration and degeneracy; imprecision in measurements; and stochasticity in modeling and simulation. In this review, we focus on the first four classes that are inherent to materials phenomena. We next develop a mathematical framework for describing materials stochasticity and then show how it can be broadly applied to these four materials-related stochastic classes. In subsequent sections, we describe structural and compositional fluctuations at small length scales that modify material properties and behavior at larger length scales; systems with engineered fluctuations, concentrating primarily on composite materials; systems in which stochasticity is developed through nucleation and kinetic phenomena; and configurations in which constraints in a given system prevent it from attaining its ground state and cause it to attain several, equally likely (degenerate) states. We next describe how stochasticity in these processes results in variations in physical properties and how these variations are then accentuated by—or amplify—stochasticity in processing and manufacturing procedures. In summary, the origins of materials stochasticity, the degree to which it can be predicted and/or controlled, and the possibility of using stochastic descriptions of materials structure, properties, and processing as a new degree of freedom in materials design are described. *Published by AIP Publishing.*

<https://doi.org/10.1063/1.4998144>

TABLE OF CONTENTS

I. INTRODUCTION	2	1. The memory effect	10
II. A MATHEMATICAL FRAMEWORK FOR STOCHASTICITY	3	2. Low loss optical fibers	11
A. Overview	3	3. High loss glasses	11
B. Forward propagation	4	C. Measurement of fluctuations and short and medium range order	11
C. Quantities of interest	5	IV. STRUCTURAL AND COMPOSITION FLUCTUATIONS: ENGINEERED	14
D. Modeling stochasticity in prediction, optimization, and inference	6	A. Composite materials	14
1. Prediction	6	V. KINETIC FLUCTUATIONS	16
2. Optimization	6	A. Nucleation phenomena	16
3. Inference	7	1. Example 1: Deformation twinning	17
III. STRUCTURAL AND COMPOSITION FLUCTUATIONS: INHERENT	7	2. Example 2: Nucleation of 2D materials during epitaxial growth	18
A. Density and composition (or concentration) fluctuation in glasses	7	3. Example 3: Recrystallization	19
B. Effects of fluctuation on glass properties	10	4. Example 4: Fatigue cracking	19
		VI. FRUSTRATION AND DEGENERACY	20
		VII. EFFECTS OF MATERIALS STOCHASTICITY ON DEVICE AND SYSTEM MANUFACTURING PROCESSES ..	21

A. Detailed example—Additive manufacturing of hierarchical fiber-reinforced soft composites	22
1. Process overview	23
2. Implications on the forcing function	24
VIII. SUMMARY AND CONCLUSIONS	25

I. INTRODUCTION

By *stochasticity* of a material, we mean inherent or engineered fluctuations in structure, chemistry, or events (such as nucleation of a defect or grain). Such fluctuations can occur over multiple length scales from the atomic to the macroscopic and can manifest themselves across both space and time. They can control the macroscopic properties of a material and define limits on materials processing and manufacturing. In special cases, they can be controlled, eliminated, or amplified to tune materials properties; in other cases, they represent a limit on the degree of control of materials performance. It is the purpose of this paper to review the manifestations of materials stochasticity and its effects on the ability to control structure, composition, properties, and manufacturability of materials. To unify the concept of stochasticity across different branches of materials sciences, we will first outline a mathematical framework to formally link the stochastic description of a material to its properties and function. We will then adopt this framework to review manifestations of stochasticity in broad fields of materials phenomena, properties, processing, and applications.

We define four broad origins of physical stochasticity in materials (1–4 below): thermodynamic, structural/compositional, kinetic, and arising from degeneracy of the phase space. Each can govern the observable properties of a material and the ability to process it into specific engineering or technological functions. We further sub-divide such fluctuations as *inherent* (i.e., arising from the intrinsic variability of the materials system) or *engineered* (i.e., arising from extrinsic manipulation of the material). The focus of this review is upon these materials phenomena. Two major additional classes of stochasticity arise from imprecisions or uncertainties in the measurement or simulation processes applied. We denote these origins as *observational* arising from finite accuracy of measurements (5 below) or *representational* associated with modeling errors/uncertainties (6 below). While closely coupled to interpretation of stochastic materials phenomena, such uncertainties in measurement and simulation are in themselves existing recognized fields, so we do not focus on them in detail in this review.

(1) *Equilibrium (thermodynamic) fluctuations.* At the most fundamental level, atomic scale fluctuations of materials are inevitable according to the laws of thermodynamics. Examples include equilibrium concentrations of point defects in a crystal or of kink densities at a surface step. Such fluctuations are stochastic because they do not localize at pre-determined site(s). They cannot be eliminated, but they can be understood and controlled through manipulation of temperature, pressure, and other state variables. Such fluctuations are *inherent*. They generally

dominate at the atomic or molecular scale and occur over time scales ranging from the fundamental time steps of atomic/molecular vibration or attempt frequencies ($ps - ns$) to the timescales of surface and bulk diffusion (s or longer).

- (2) *Structural/composition fluctuations.* Fluctuations in structure and composition arise from multiple origins and can occur over multiple length scales. They can be *inherent* or *engineered*. Examples include *inherent* fluctuations in the local composition of glasses or of miscible crystalline alloys at the sub-nm scale, *engineered* variations in thin film multilayers through advanced planar growth techniques at length scales of angstrom— μm , and *engineered* variations in a matrix/particle composite material at length scales of nm—mm.
- (3) *Kinetic fluctuations.* The growth, synthesis, and processing of materials into a useful engineering or technological form involves a time-series of phenomena that are *inherently* stochastic, but that can be controlled or *engineered* through judicious choice of processing conditions. Examples include precipitate or grain nucleation and phase transformations. Such events typically involve activation of a process over an energy barrier and occur over broad ranges of length and time scales, from nm to mm, and ns to hours or even years. While the energetic framework governing these events can generally be defined, the stochastic nature of individual nucleation or transformation events generally cannot.
- (4) *Frustration and degeneracy.* An additional route to stochastic system behavior occurs when the ground state of a system is highly degenerate, and the system has to randomly choose between multiple states that are equivalent (or quasi-equivalent—i.e., within energy differences $\sim kT$) energetically while showing high structural differences. Such fluctuations are *inherent*. A prototypical example of this effect is in small metallic clusters, where the number of isomers increases rapidly with the number of atoms. Because formation energy differences can be less than kT for large number of these isomers, it is difficult to predict the ground-state unequivocally. In this case, ensemble averages satisfactorily represent properties of a single structure. A related concept is that of structural frustration, whereby the equivalence of multiple system states causes the evolution of relatively complex structures as system components evolve from multiple equivalent configurations. These coupled phenomena can cause equivalent systems to diverge along an unlimited number of pathways, thereby creating stochasticity.
- (5) *Imprecision in measurement.* The relationship between the true stochastic nature of material, or its evolution in time, and the observed description of that material is not exact. Rather, it is governed by *observational* limitations, defined by the instrumental transfer function. Examples include the spatial resolution of a particular technique at one limit of structural length scale or the field of view at the opposite limit of structural length scales. If the fluctuations in a structure occur at length scales finer than the spatial resolution, they will be averaged out in the observation. If they occur at length scales

greater than the field of view, they will not be sampled. In both cases, the stochasticity is not apparent to the observer. Similar limitations occur in the time domain, where the signal acquisition time may be larger than the timescale over which individual kinetic events occur or events may occur over impractically long time scales for measurement. We do not focus in depth on such observational limitations in this review, because while they contribute to the stochasticity in interpreting materials phenomena, they are not in themselves a direct cause of stochastic material behavior, which is the focus of this review. Existing relevant treatments include established methods of error analysis (e.g., Ref. 1), thorough analysis of the set of experimental variables that can affect the interpretation of materials structure/chemistry in a specific characterization experiment (e.g., Ref. 2), to artificial intelligence treatments of most likely structures under a given set of experimental measurement parameters (e.g., Ref. 3).

- (6) *Stochasticity in modeling and simulation.* Computation of materials structure, composition, properties, and phenomena will be limited by the accuracy of the fundamental descriptions and physical models embodied into the simulation code and the degree to which we can solve these models, leading to *representational* stochasticity. Here, we must separate the errors related to the theory itself and those arising from its actual algorithmic implementation. Examples of model errors can be as fundamental as missing entire physics phenomena, to deficiencies in the modeling parameters such as imprecision in atomic bonding potentials for structure prediction, or in exchange integrals for prediction of magnetic properties, or in the algorithmic compromises necessary to access computation that are necessary to access sufficiently large length or time scales. Since models are mathematically defined in an infinite dimensional space and our ability to compute is finite, there will be errors of approximation due to our finite discretization of the model. There are also sources of errors due to the fact that the computations are of finite precision, leading to numerical round off which can potentially destroy the value of a calculation. A specific opportunity and challenge in computational description of stochasticity relates to the ability to consider the influence of models across multiple time and space scales through the application of multi-scale linkage. This is an opportunity in that this ability to simulate behaviors across scales can provide critical insights into the ability to control materials. It is also a critical challenge in that the models and computational methods to link across scales are not well understood and are difficult to verify and more difficult to validate—largely absent in experimental observation—is how the “errors” at one computational length/time scale propagate—and potentially amplify—into descriptions at other length/time scales. We do not focus in depth on such computational limitations in this review, because while they contribute to the stochasticity in predicting materials phenomena, they are

not in themselves a direct cause of stochastic material behavior, which is the focus of this review. Extensive established methods exist for treatment of stochasticity in computation, and the main approaches are briefly summarized in Sec. II of this review.

These six classes of stochasticity can be classified as being *aleatory* or *epistemic*. Aleatory uncertainties are intrinsic to a system and cannot be reduced with any amount of measurement or data. These include categories (1) (thermodynamic), (3) (kinetic), and (4) (frustrative) above. Category (2) (structural/compositional fluctuations) are also aleatory when inherent to the system. Epistemic uncertainties, on the other hand, represent our lack of knowledge or data within a system. These can often be reduced with more measurements or better characterization. These include categories (5) (measurement), (6) (computation/simulation), and (2) (when engineered).

This review is structured as follows. In Sec. II, we provide a mathematical framework for describing stochastic structures and resultant properties (a reader who wishes to directly move to the materials manifestations of stochasticity that we describe can move straight to the subsequent sections). In Sec. III, we focus on structural/compositional fluctuations (mainly inherent), i.e., origin of stochasticity number 2 above, specifically short-medium structural, compositional, and density fluctuations in glasses. In Sec. IV, we examine engineered composite structures (another subset of stochasticity origin 2 above), and how order parameters and correlation lengths in such materials may be used to tune both local and macroscopic properties. In Sec. V, we consider examples of microstructural and mechanical property variations that arise from kinetic stochasticity (origin number 3 above)—events that are stochastic in time and space—focusing on nucleation, recrystallization, deformation twinning, and fatigue cracking. In Sec. VI, we examine systems where stochasticity arises from distributions of material units across a set of states that are equivalent in energy, i.e., frustrated systems (origin number 4 above). In Sec. VII, we discuss the role of stochasticity in an exemplary advanced manufacturing process, fabrication of laminated polymer nanocomposite 3D structures, where variations in the material parameters of individual components, as well as variations in process parameters, lead to a nano-composite with stochastic microstructure and hence stochasticity in its macroscopic physical properties.

II. A MATHEMATICAL FRAMEWORK FOR STOCHASTICITY

A. Overview

In the Introduction, we have described the different sources of uncertainty (stochasticity) in materials based on their physical origins. To help understand the influence these sources of uncertainty have on the resulting behavior of materials systems, it is important to quantify them to the best of our ability. This necessitates a framework to understand these sources and ultimately to control them to produce the desired structures and properties. Here, this challenge is addressed in the context of a mathematical framework that

lays the foundations for simulating materials accounting for stochastic behavior. Figure 1 shows the generic structure of this framework. The link between structure and performance is provided by a forward propagator. The propagator represents the fundamental balance laws that govern the material behavior of interest and includes the constitutive information. The propagator may contain several parameters, such as material property parameters or parameters of an interatomic potential, etc. In addition to this propagator, which is typically represented by an algebraic or a (partial) differential equation, there are additional data like initial and boundary conditions, and forcing functions that are necessary to yield a mathematically well-posed system of equations. The forcing functions represent the interaction of the system modeled with fields or perturbations that are not explicitly represented in the model. Thus, there are two classes of parameters and fields that arise naturally: those associated with the forward propagator itself, and those associated with the additional data that are required to ensure that the problem is well-posed. Uncertainty in any of these parameters/fields leads to a stochastic system. As a result, from the perspective of modeling a material system, the relevant sources of uncertainty are

- (a) Uncertainties in the parameters and fields in the forward propagator: In a continuum system, these would be the material parameters like thermal conductivity, elastic-visco-plastic moduli, etc. In models for chemical reactions, these could be expressions for reaction rates.
- (b) Uncertainties in accompanying data: these include (i) initial data: for example, the uncertainty in the initial state of an MD system or experimental glassy system,

(ii) boundary data: for example, uncertainty in the temperature boundary condition for a thermal problem, and (iii) forcing data: for example, uncertainty in the forcing term that represents the effect of sub-scales in a coarse grained discrete simulation.

In addition to these sources, there is the uncertainty in the model itself, i.e., in the nature of the forward operator. This arises because any given mathematical model describes a physical process based on a combination of mathematical principals, basic “physics laws,” observed behavior and limited experimental information. Ultimately, there are assumptions, including missing physics, and simplifications embedded in a model that introduce error in its predictions (see Ref. 4 for an application of this idea in climate modeling). This error is termed model error, and in many cases, it is represented as a stochastic process that contributes to the uncertainty in the model prediction. In addition, there are potential errors associated with the discretization of that model and execution of finite precision calculations. For purposes of the discussion presented in this paper, it is assumed that these errors are explicitly controlled to be small compared to the potential modeling errors. The reason for this assumption is that there are methods available to exercise control of these errors.⁵ In reality, in real world simulations, these methods are not necessarily applied to the level they should be.

B. Forward propagation

The trajectory taken by a system in phase space is defined by applying a set of boundary and initial conditions to a forward operator that represents the physics of the

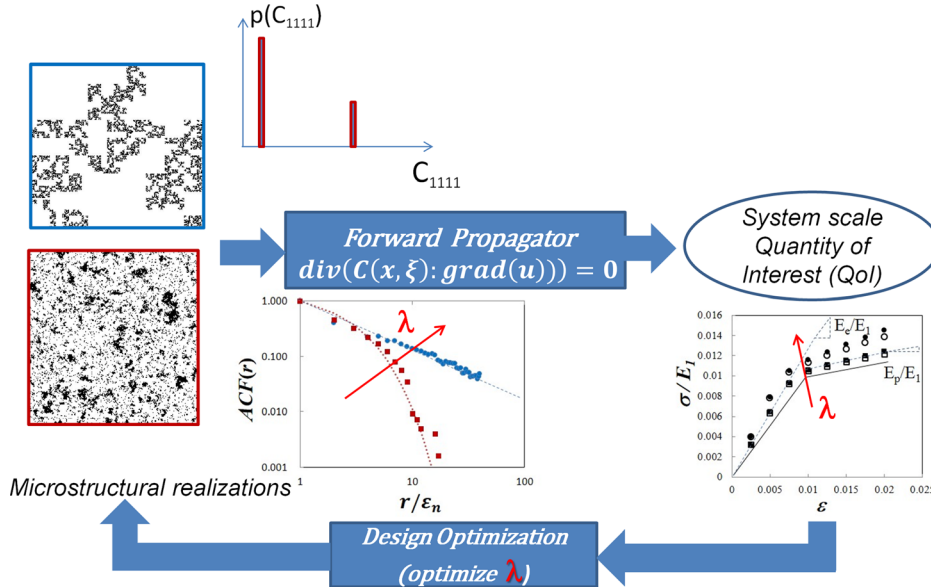


FIG. 1. Schematic representation of ways to account for stochasticity in the mathematical description of material behavior. Multiple realizations of a random microstructure subjected to potentially stochastic initial and boundary conditions and to forcing functions are evaluated by forward propagation with a physically relevant operator. The output is used to evaluate quantities of interest. The framework developed in this article is suggested by the control loop shown which indicates an optimization of the output based on controlling the stochastic parameters of the initial problem. An example is provided related to composite materials with stochastic microstructure.⁶ The control parameter selected is the correlation length of the spatial distribution of inclusions, λ , defined by the autocorrelation function $ACF(r)$. The volume fraction of inclusions is identical in the two realizations, as suggested by the probability distribution function of elastic constants, $p(C_{1111})$. The stress-strain curve is taken here as the quantity of interest and is obtained by solving a boundary value problem defined by the forward operator specific to mechanics. The quantity of interest is sensitive to the control parameter λ .

problem. This operator generates the fields of interest, which evolve in time.

In general, one may write the forward operator as

$$\{\mathfrak{I}(\mathbf{U}(\mathbf{x}), \mathbf{C}(\xi), \eta) = 0, BIC(\zeta)\}, \quad (1)$$

where \mathfrak{I} acts on the generic field of interest \mathbf{U} and a set of problem-specific parameters, \mathbf{C} . These are material constants such as thermal conductivity, diffusivity, or elastic constants and may be stochastic functions of the random variables in the set ξ . The operator itself may be stochastic, which is expressed by making \mathfrak{I} an explicit function of another set of random variables, η . The operator evolves \mathbf{U} within the restrictions imposed by the boundary and initial conditions (BIC), which may also contain stochastic terms, ζ . The various sets of random variables may be independent or correlated. The solution field \mathbf{U} is therefore dependent on all random variables used in the definition of the problem and on the spatial and temporal coordinates \mathbf{x} .

To exemplify this, let us consider a heat transport problem in a generic material context. In this problem, the operator \mathfrak{I} is applied to the scalar temperature field, $U \equiv T$, and is defined by

$$\mathfrak{I} \equiv c\rho \frac{\partial T}{\partial t} + \text{div}(\kappa \text{grad} T) + Q = 0, \quad (2)$$

where the scalar fields κ , c , and ρ are material parameters, being, respectively, the thermal conductivity, the specific heat, and the density. Note that the operator in Eq. (2) is deterministic and hence variables η in Eq. (1) are absent in Eq. (2). The equation is derived based on the equation of conservation of thermal energy

$$c\rho \frac{\partial T}{\partial t} - \text{div} \mathbf{j} + Q = 0, \quad (3)$$

and the linear relation (constitutive law) between the heat flux, \mathbf{j} , and the gradient of temperature, $\mathbf{j} = -\kappa \text{grad} T$. The material parameters form the parameter set \mathbf{C}

$$(\mathbf{C}(\xi) = \{\kappa(\xi), c(\xi), \rho(\xi)\}). \quad (4)$$

This set may be position dependent and may also be a function of the stochastic variables ξ . The source term Q may also be deterministic or a function of stochastic variables.

We also note that the potential whose gradient provides the thermodynamic driving force for the process may be non-convex, which may lead to phase separation and patterning, as well as to degenerate states (as detailed in Sec. VI). The effect of the stochastic terms of the governing operator on this phase separation process is of interest in many problems, especially close to critical points.

Another example frequently used in materials science problems is that associated with the second law of Newtonian dynamics used in Molecular Dynamics models. In this case, the operator \mathfrak{I} is applied to a discrete set of variables representing the positions of particles, $\mathbf{U} \equiv \{x_i, i = 1 \dots N\}$

$$\mathfrak{I} \equiv m_i \frac{\partial^2 x_i}{\partial t^2} + \frac{\partial W(\mathbf{x})}{\partial x_i} = 0. \quad (5a)$$

Here, m_i is the mass of the i -th particle and W is the potential energy of the system. The stochastic parameters in this problem are related to the initial conditions, while the operator is deterministic.

Mapping the atomistic model into a coarse grained representation of the same system of particles entails the introduction of stochastic terms in the forward operator \mathfrak{I} .^{7,8} Specifically, the resulting Langevin equation has a dissipative term, $\chi \frac{\partial x_i}{\partial t}$, and a random term, $R(t)$, in addition to the inertia and deterministic driving terms shown above, Eq. (5a), i.e.,

$$\mathfrak{I} \equiv m_i \frac{\partial^2 x_i}{\partial t^2} + \frac{\partial W(\mathbf{x})}{\partial x_i} - \chi \frac{\partial x_i}{\partial t} + R(t) = 0. \quad (5b)$$

The two new terms are related to each other through the fluctuation-dissipation theorem and represent the energy exchange between the degrees of freedom of the coarse grained model and the thermal bath of the variables eliminated during coarse graining.

Examples of the appropriate forward operators will be described in subsequent sections on specific manifestations of stochasticity.

C. Quantities of interest

The quantity of interest (QoI) in a specific application may be either the field \mathbf{U} predicted by the forward operator, a function of \mathbf{U} representing, for example, an average quantity, or an extremum of \mathbf{U} . One can write, in general: $QoI = \mathcal{A}(\mathbf{U})$, where, as above, \mathbf{U} is position and time dependent and is also a function of the stochastic variables of the problem. Operator \mathcal{A} can take many forms and describes whether the QoI is global (e.g., an average over the entire problem domain) or local (e.g., an L^∞ norm which provides the maximum of the field).

Averaging operators generally have the form

$$QoI = \frac{1}{V} \int_V f(\mathbf{U}) dV. \quad (6)$$

Here, V is the volume of the problem domain or the relevant subset of it, and f is a function related to the nature of the QoI. For example, focusing on an example of an *engineered* stochastic material defined in the Introduction, when studying a composite material, one may be interested in the tangent modulus which is computed as the stress increment corresponding to an imposed strain increment. The stress increment is computed as an average of the local stress in the composite. Then, f represents a time/strain differential operation and \mathbf{U} represents the stress field. Incorporating plasticity, for example, through a Discrete Dislocation Dynamics (DDD) model, one may be interested in determining the total plastic strain associated with an increment of the applied stress. The DDD model is a discrete model in which all dislocations present in the volume of material considered are explicitly represented and their motion and interaction are captured. The forward operator predicts in this case the displacement of each dislocation segment. The plastic strain increment is computed as the sum of contributions of

dislocation segments moving in all slip systems. Hence, the QoI is effectively an average over the entire population of dislocations.

The QoI may be also related to the local values of the fields. In this case, operator \mathcal{A} filters the information contained in \mathbf{U} , leading to quantities that are relevant locally. For example, in problems in which damage nucleation is important, one is interested in identifying those regions of the material in which a certain quantity, for example, the total accumulated plastic strain, or the maximum principal stress, reaches values above a specified threshold. In such problems, the mean of \mathbf{U} is less important than the right tail of the distribution of \mathbf{U} (large values of \mathbf{U}).

The objective of solving the forward problem in the presence of *stochasticity* is thus to predict the distribution function of the QoI. If \mathcal{A} is of the averaging type, it is expected that the QoI distribution is significantly narrower than that of \mathbf{U} . However, if \mathcal{A} is of maximum (or minimum) norm type, the tail of the distribution of \mathbf{U} matters.

D. Modeling stochasticity in prediction, optimization, and inference

The overall objective of any modeling exercise is typically (a) to create a predictive model for a certain QoI, or (b) to determine the values of parameters that will optimize a certain QoI, or (c) to infer the state of the system by comparing the computed and the observed values of a QoI.

1. Prediction

Predictive science and engineering involve three essential ingredients.⁹ These are experimental observations, mathematical models derived from physical principles, and computational approximation of these models. Each of these ingredients includes and introduces stochastic variations that have been summarized in Sec. II A. These uncertainties are propagated from the input variables to the quantities of interest, leading to the stochastic description of the QoI. This process has the structure of a typical forward problem where information and uncertainty are propagated from the input parameters to the QoIs.

Perhaps the simplest computational methods for solving the stochastic forward problems are sampling techniques like the Monte-Carlo method, where samples of input parameters are drawn and the forward problem is solved as if it was a deterministic problem to generate realizations of the QoI. These realizations are then used to evaluate statistics of interest. Though this approach is very simple and has the benefit of using an existing deterministic code as a “black-box,” it suffers from slow convergence. For example, using this method, the error in computing the mean of a quantity reduces as $\sim 1/\sqrt{N}$, where N is the number of samples. We note that many methods have been proposed to accelerate this convergence, and this field continues to be an active area of research.^{10–12}

A relatively new class of methods for solving the stochastic forward problem relies on expanding the solution, or the QoI, in terms of a generalized polynomial chaos (gPC)

expansion.¹³ The specific form of the polynomial series is determined by the probability distribution function (pdf) of the random input parameters. Using this expansion amounts to using a spectral approximation for the solution and leads to exponential convergence rates, which in turn reduce the effort needed to determine the QoI. There are two major classes of gPC methods. Stochastic Galerkin methods lead to large-scale coupled problems and require the development of codes that are designed specifically for solving stochastic problems.^{14–16} Since these methods entail the reworking of existing deterministic codes, they are often also referred to as intrusive methods. In contrast to this are the gPC methods based on stochastic collocation. These methods lead to an “optimal” sampling strategy and are described as non-intrusive, because like the MC methods they use an existing deterministic code like a black-box within a clever sampling strategy.^{17,18}

2. Optimization

Often one is interested in determining the values of a set of parameters that will optimize a specific QoI or combinations of QoIs. When the QoI is deterministic, this leads to a deterministic optimization problem. There are many ways to solve this problem, and the choice of an appropriate method is determined by factors such as the smoothness of the dependence of the QoI on the parameters, the number of parameters, and the constraints imposed on the system. Most optimization methods involve the selection of a trial state of parameters, evaluation of the QoI and other variables (sensitivities, for example) at this state, and an update to the state based on these values. This process is repeated until convergence. Thus, when solving an optimization problem, the flow of information is no longer open ended, but is in the form of a loop that is performed until the desired solution is attained (see Fig. 1).

When the QoIs are stochastic, one is led to a stochastic optimization problem. In this case, it becomes necessary to specify the statistic of the QoI that needs to be optimized. The simplest example of a common statistic is the expectation. For example, consider a composite material with a stochastic microstructure, where the QoI is the coarse-scale tangent modulus. Since the microstructure is stochastic, this modulus will also be a stochastic variable. An appropriate optimization problem is then to determine the microstructure that would maximize the expected value of the coarse-scale tangent modulus. Note that it no longer makes sense to optimize the modulus itself, we have to optimize its statistic, in this case, its expected value. Another variant of this optimization problem that emphasizes robustness is: determine the microstructure that would yield a modulus that is greater than a threshold value while minimizing the variance in modulus.

The algorithms for solving stochastic optimization problems are motivated by those used for their deterministic counterparts and also require the flow of information and uncertainties in a closed loop as described in Fig. 1. These algorithms include methods like stochastic approximation,

the stochastic gradient descent method, and scenario optimization.^{19–21} Remarkably, some of these methods, like the stochastic gradient descent method, are also efficient and robust methods for solving deterministic optimization problems and are widely used in machine learning applications.

3. Inference

In an inference problem, one utilizes the measurement of observed QoIs to determine the values of some other parameters of the system. These types of problems are also referred to as inverse problems, since the measured QoIs are often the outputs of a predictive model and the parameters that are sought are the inputs. Inference problems may be solved as an optimization problem where the values of the parameters of the system that minimize the discrepancy between the measured and predicted QoIs are sought. This approach has analogies to methods of evolutionary biology, where phylogenetic sequences are derived from Bayesian methods where the posterior distributions of data inform the evolutionary model.

When the parameters of the system and/or the QoIs are stochastic variables, one is naturally led to a stochastic inference problem. A recent trend in solving stochastic inference problems—in both physical and biological sciences—relies on the Bayesian interpretation of probability.²² Using this interpretation, a probability is assigned to propositions (inference), and these probabilities are determined using the so-called Bayesian methodology. Within this approach, a prior probability is attached to the outcome of an inference, which depicts our current belief about the proposition, and this probability is updated in the light of new measurements by making use of Bayes rule leading to the definition of a posterior-probability for the inference. The implementation of this approach involves a large-scale sampling problem where the posterior-probability must be judiciously sampled in order to evaluate statistics of the inferred parameters. The Markov-chain Monte-Carlo (MCMC) method and its variants are the most popular methods for solving this sampling problem.^{23–25} This involves repeated solution of the forward problem, and this framework is similar to the closed-loop flow of information and uncertainties observed in optimization problems.

In summary, the main utility of evaluating a QoI is either its prediction, or its optimization, or its use in inferring a related parameter. When the QoI is a random variable, then the corresponding prediction, optimization, and inference problems become stochastic, and formulations and methods that acknowledge this stochasticity are required. Further, both optimization and inference problems are typically solved in an iterative scheme where the current estimate of a QoI is used to set up a new forward problem for the propagation of information and uncertainties, which then leads to a new estimate of the QoI and so on. These concepts are relevant to the following sections: In Sec. III, where we describe structural and composition fluctuations at small length scales that modify material properties and behavior at larger length scales, the stochasticity is embedded in the distribution of parameters of the forward operator, and it directly influences

the quantities of interest, which are material properties at a coarser scale. Specifically, the stochastic fluctuations in the density and composition fields of glasses determine the memory effects and optical absorption at larger length scales. In Sec. IV, which considers systems with engineered fluctuations, we concentrate primarily on composite materials where the quantities of interest are typically mechanical properties and the forward operator relates the stochasticity in the distribution of inclusions in the matrix to the global mechanical properties. In Sec. V, where we consider nucleation and kinetic phenomena in materials, stochasticity is introduced via the parameters of the forward operator. Typically, the quantity of interest in this case is best represented by a maximum-type (L^∞) norm since damage nucleation is controlled by maxima of local field fluctuations. The problem involves a criterion that links these fluctuations to the probability of nucleation. This probabilistic function introduces additional stochasticity that is associated with physical processes not explicitly represented in the problem description. In Sec. VI, we consider the case where constraints in a given system prevent it from attaining its ground state and cause it to attain several, equally likely (degenerate) states. In this case, randomly selected initial states or random forcing functions can be used to statistically sample and characterize the solution space. Finally, in Sec. VII, we discuss the role of stochasticity in an exemplary advanced manufacturing process. Here, the forcing functions represent interactions of the system with fields or perturbations that are not explicitly represented in the model. These forcing functions comprise both deterministic as well as stochastic components. The deterministic components originate from the repeatable/controllable aspects of the manufacturing process, whereas the stochastic components come from inherent fluctuations in the process variables that are outside the purview of closed-loop process control.

III. STRUCTURAL AND COMPOSITION FLUCTUATIONS: INHERENT

In this section, we focus on the origin of stochasticity number 2 in the Introduction, where stochasticity arises from random or incompletely correlated short-medium range fluctuations in materials and modifies materials properties. Examples are provided from compositional and density fluctuations in glasses.

A. Density and composition (or concentration) fluctuation in glasses

The structures of many glasses are known to fluctuate, in both composition and density, at length scales of order a nanometer. Such fluctuations can control many of the observable properties of glasses. It is useful to define the concept of *fictive temperature*²⁶ to explain the fluctuation in glasses. Figure 2 shows a schematic diagram of the specific volume of a glass-forming system vs. temperature. When a glass forming liquid is cooled slowly, e.g., at 20 K/min, its specific volume decreases following the extension of the liquid line, even when temperature becomes lower than the melting (or freezing) point, T_m . When the liquid is cooled

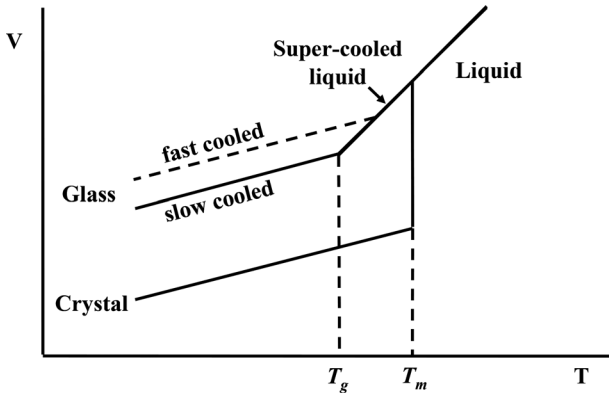


FIG. 2. Specific volume of a glass-forming system as a function of temperature.

further, at some low temperature, the specific volume starts to deviate from the extension of the liquid line. This temperature of the deviation is the glass transition temperature, T_g . Between the two temperatures, T_m and T_g , the material is super-cooled liquid and is in a metastable equilibrium state. When the liquid is cooled at a faster rate, the point of the deviation occurs at a higher temperature as indicated by the broken line in Fig. 2. This cooling rate-dependent glass transition temperature is called a fictive temperature of the glass and the glass is assumed to retain the structure of liquid frozen at the fictive temperature. Thus, different glass samples with the same composition can have different fictive temperatures depending upon the cooling rate. For example, a pure silica glass block has the fictive temperature near the glass transition temperature, 1200 °C, but a silica glass optical fiber can have a much higher fictive temperature, e.g., ~1650 °C, because the silica glass fibers are made by rapid cooling of molten silica glass. It is important to realize that when a glass sample is brought to its fictive temperature instantaneously, the glass would be in a metastable equilibrium state. The fictive temperature of a glass sample can vary with time when the sample was heat-treated at a temperature near the glass transition temperature, but it remains unchanged at low temperature, e.g., room temperature.

Diagrams such as Fig. 2 can also inform other glass properties, such as enthalpy and the extent of density

fluctuations. The latter is revealed, for example, by light scattering and small angle X-ray scattering (SAXS) intensities. Figure 3 shows SAXS intensities extrapolated to zero angle for (a) silica glass and (b) soda-lime silicate glass samples having different fictive temperatures as a function of temperature.²⁷ The glass samples employed for these scattering measurements were held at various temperatures, in the glass transition temperature range, for a sufficient time to reach a metastable equilibrium state and rapidly cooled. By this procedure, the fictive temperature of glass samples becomes same as the heat-treatment temperature.

A glass, being a frozen liquid, retains the structure of liquid in which component atoms and molecules were constantly moving. As a liquid is cooled continuously, its viscosity increases and the atomic or molecular motion in liquid gradually becomes sluggish and eventually stops completely and the liquid would turn into a glass. The extent of fluctuation of a glass would therefore vary with the fictive temperature of the glass, reflecting the structure of the liquid at the fictive temperature. *The fictive temperature is thus a very effective surrogate for the degree of stochasticity in the glass structure.* All glasses, including a single component glass, e.g., pure SiO₂, can have density fluctuations, while multi-component glasses can have, in addition to the density fluctuation, composition fluctuation.

For a system in equilibrium at temperature T, the density fluctuation of a liquid can be given by^{28–34}

$$\frac{(\Delta\rho)^2}{\rho_0^2} = \frac{1}{V} \beta_T(T) kT, \quad (7)$$

where ρ is the local density, ρ_0 is the average density, $\Delta\rho = \rho - \rho_0$, $(\Delta\rho)^2$ is the average of $(\Delta\rho)^2$, β_T is the isothermal compressibility, k is the Boltzmann's constant, and V is the volume of the fluctuation. The temperature dependence of zero angle SAXS intensity of silica glass in the low temperature region appears independent of fictive temperature according to Fig. 3(a). Thus, zero angle SAXS intensity determined at room temperature can be used as a measure of the fictive temperature effect on density fluctuation of silica glasses. Figure 4 shows the linear dependence of zero angle

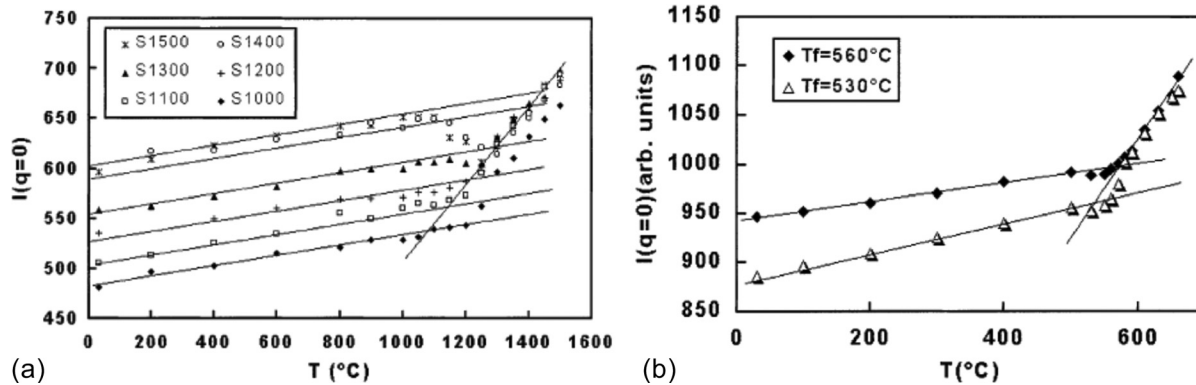


FIG. 3. (a, left) Zero angle SAXS intensity of SiO₂ glass samples with different fictive temperatures plotted as a function of temperature of measurement. The S numbers indicate the fictive temperature (°C) of silica glass. (b, right) Zero angle SAXS intensity of soda-lime silicate glass samples with different fictive temperatures plotted as a function of temperature of measurement. T_f values are fictive temperature of the samples. Reproduced with permission from Levelut *et al.*, J. Non-Crystalline Solids 307–310, 426 (2002). Copyright 2003 Elsevier.

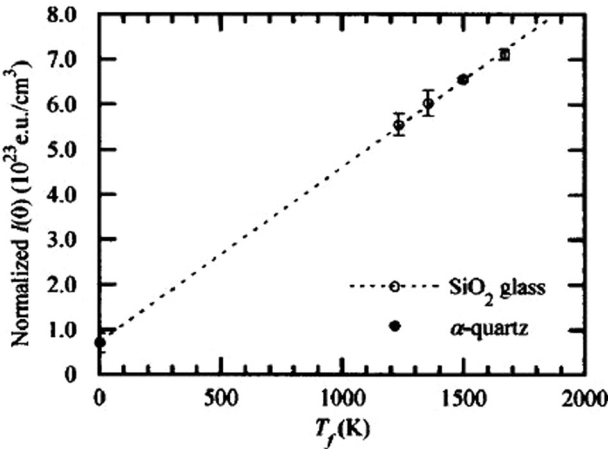
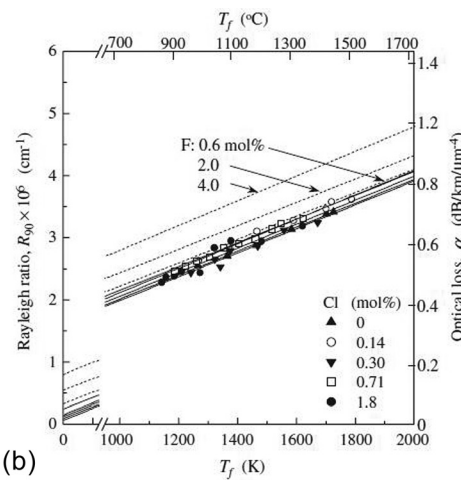
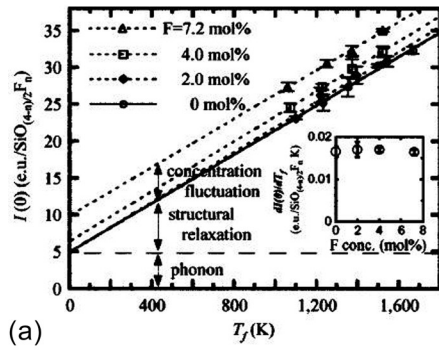


FIG. 4. Zero angle SAXS intensity at room temperature of silica glass as a function of fictive temperature. The value for α -quartz was calculated and plotted at $T_f=0$. From J. Appl. Phys. **94**, 4824 (2003). Copyright 2003 AIP publishing LLC.

SAXS intensity on T_f^{34} for pure silica glasses. The value extrapolated to zero T_f appears to agree with the SAXS intensity of α -quartz, a crystalline form of SiO_2 . It has been reported that zones in silica glass of $\sim 20 \text{ \AA}$ in diameter appear to have a structure similar to that of a crystalline SiO_2 phase, cristobalite.³³

The scattering method to measure the fluctuation can be extended to silica glasses with trace amounts of additives. Figure 5(a)³⁵ shows the SAXS intensities for silica glasses with various concentrations of fluorine, F, plotted against the fictive temperature of the samples. A parallel shift upward of the scattering intensities with increasing F contents indicates that F-containing silica glasses have *concentration fluctuations*, in addition to the density fluctuation, and the concentration fluctuation increases with increasing F contents. In contrast, Fig. 5(b)³⁶ shows the 90° Rayleigh scattering intensity changing very little with Cl-contents of silica glasses indicating that there is little concentration fluctuation in these silica glasses.

The composition fluctuation usually has the opposite fictive temperature dependence to the density fluctuation, since at higher temperature a glass homogeneity improves. It is also highly dependent on glass compositions, in particular,



on the composition dependence of the Gibbs free energy, G, since it is given by the following relation:³⁷

$$\overline{(\Delta C)^2} = \frac{kT}{\left(\frac{\partial^2 G}{\partial C^2}\right)_{T,P,N}}. \quad (8)$$

Here, C is local concentration and, for a binary system, is given by $C = N_1/(N_1+N_2)$, where N_1 and N_2 are the number of molecules in a volume V of components 1 and 2, respectively, and $N = N_1+N_2$, and $\Delta C = C - C_0$ and C_0 is the average concentration. This expression shows that the concentration fluctuation is closely related to the position of glass-in-glass immiscibility boundary, since at the critical point $(\frac{\partial^2 G}{\partial C^2})_{T,P,N} = (\frac{\partial^3 G}{\partial C^3}) = 0$ and at spinodal $(\frac{\partial^2 G}{\partial C^2})_{T,P,N} = 0$ concentration fluctuation becomes infinity.

In general, it is expected that even a homogeneous glass can have an immiscibility boundary at lower temperatures, although the phase separation cannot be achieved due to kinetic reasons. Composition fluctuations in a homogeneous glass can become greater if the temperature is lowered and approaches the critical temperature or the spinodal line of the immiscibility boundary. Simmons *et al.*³⁸ observed that a homogeneous $\text{Na}_2\text{O}-\text{B}_2\text{O}_3-\text{SiO}_2$ glass exhibited a higher viscosity than the extrapolated value from higher temperatures, at just above the critical point of the immiscibility boundary. This can be attributed to large value of $\overline{(\Delta C)^2}$, due to a small value of the denominator of Eq. (8) approaching zero. The glass composition would consist of a region of high silica content and a region of low silica content, probably with interconnected microstructure, and the resulting high viscosity of high silica region would dominate viscosity of the glass producing a higher viscosity observed.

When two homogeneous glass compositions are compared at the same temperature, the system with a higher critical temperature is expected to have a greater concentration fluctuation, since the system would be closer to the critical temperature and the denominator of Eq. (8) would be closer to zero. Some alkali silicate glass systems exhibit immiscibility boundaries with the higher immiscibility temperature being observed for $\text{Li}_2\text{O}-\text{SiO}_2 > \text{Na}_2\text{O}-\text{SiO}_2 > \text{K}_2\text{O}-\text{SiO}_2$.³⁹ The higher immiscibility tendency was attributed to the

FIG. 5. (a) Zero angle SAXS intensity at room temperature of SiO_2 glasses with different F contents as a function of fictive temperature. The inset shows the values of the slopes of lines and indicates the lines have same slopes. From J. Appl. Phys. **95**, 2432 (2004). Copyright 2004 AIP publishing LLC. (b) Rayleigh scattering intensity at 90° measured at room temperature for SiO_2 glasses with various Cl contents as a function of fictive temperature. Reproduced with permission from Kakiuchida *et al.*, Jpn. J. Appl. Phys., Part 2 **42**, L1526 (2003). Copyright 2003 The Japan Society of Applied Physics.

higher ionic field strength of component ions, $\text{Li}^+ > \text{Na}^+ > \text{K}^+$.⁴⁰ By analogy, it is expected that the F-containing silica system would have a greater tendency of immiscibility than Cl-containing silica glass system. This is probably the reason why the higher concentration fluctuation was observed in F-containing silica glasses, while practically no concentration fluctuation was observed for Cl-containing silica glasses.

The extreme case of composition fluctuation of glass is glass-in-glass phase separation,³⁹ which takes place inside the immiscibility boundary, where two different glass compositions are separated, just as two liquids such as water and oil separate, except that kinetics of glass-in-glass phase separation is much slower and its developed microstructures are usually much finer than those of liquids. These glass-in-glass phase separations are defined by immiscibility boundaries. An example of glass-in-glass immiscibility boundary is shown for the $\text{SiO}_2\text{-Na}_2\text{O}$ systems in Fig. 6(a), together with the developed microstructures shown in Fig. 6(b).⁴¹ Glass-in-glass phase separated glasses are similar to composite materials and they have different properties from the homogeneous glass composition. Optical properties of phase separated glasses, for example, vary depending upon the size of microstructure. When the size of microstructures is small, the glass can exhibit faint opalescence and its color darkens as the size of microstructure increases, eventually becoming opaque. Many other properties such as chemical durability, mechanical strength, and electric conductivity vary with their microstructures.

B. Effects of fluctuation on glass properties

A specific theme of this review is how stochastic variations in structure, composition, and microstructure can control materials properties. In this section, we discuss how glass properties are affected by compositional and density fluctuations, with specific examples of the “memory effect,” engineering lower loss optical fibers, and high loss materials.

1. The memory effect

Most glasses exhibit the memory effect, in which they behave as if they remember their thermal history. For example, glass samples having different thermal histories but identical composition and properties would behave differently, exhibiting different property changes upon a subsequent heat-treatment. This phenomenon has been observed in all types of glasses including oxide glasses,⁴² polymeric glasses,⁴³ and metallic glasses,⁴⁴ and attributed to fluctuations within the glass, with different regions having different relaxation times. The overall property change in the glass is determined by the combinations of property changes at different rates at the different regions. Even when two samples of the same glass had the same apparent property, their individual regions may have different properties. Upon a subsequent heat-treatment, these individual regions can change at different rates, producing different manner of property changes for two samples with different thermal history. These different regions may have different extents of density fluctuation or composition fluctuation.

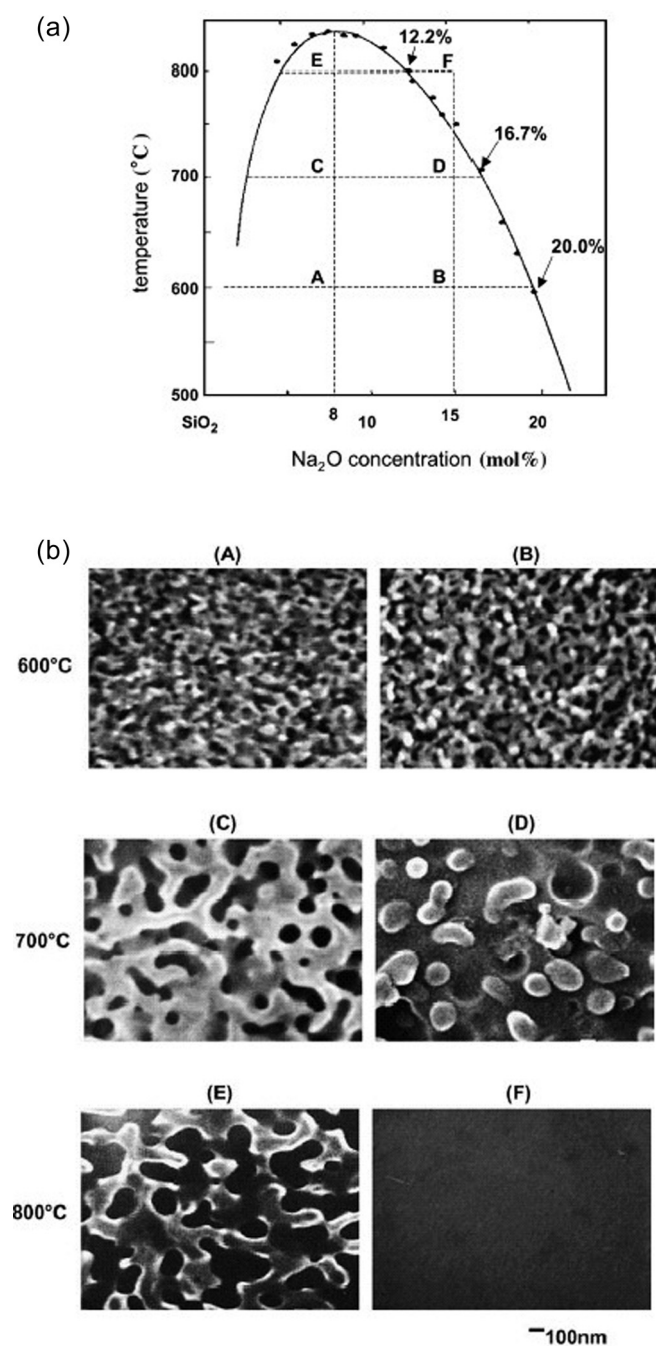


FIG. 6. (a) Metastable immiscibility boundary of $\text{Na}_2\text{O}\text{-SiO}_2$ glass system. (b) SEM images of glass-in-glass phase separated microstructures of $\text{Na}_2\text{O}\text{-SiO}_2$ glass system developed by heat-treatment at selected temperatures of selected glass compositions. These selected points are indicated in (a). Heat-treatment conditions were 800 °C, 4 h; 700 °C, 16 h; and 600 °C, 30 h. Reproduced with permission from Fujita *et al.*, J. Non-Cryst. Solids 328, 64 (2003). Copyright 2003 Elsevier.

Since the memory effect was observed even for a single component glass such as high purity B_2O_3 glass,⁴⁵ the effect has been traditionally attributed to density fluctuation. Recently, the memory effects of silica glass with various impurities such as OH, F, and Cl were investigated. It was found that the memory effect was observed for SiO_2 glasses containing impurity OH or F, but not for silica glass with impurity of 1000 ppm Cl.⁴⁶ This difference can be attributed to the different composition fluctuation characteristics of

these silica glasses. OH in silica glass is expected to produce a large composition fluctuation, in view of the well-known immiscibility boundary in the H₂O-SiO₂ system. Figures 5(a) and 5(b) showed that F-doped silica glass exhibited the concentration fluctuation, while Cl-doped silica glass did not. From these observations, one can speculate that the memory effect of silica glasses was caused by concentration fluctuations, rather than density fluctuations. The question remains, then, why a high purity B₂O₃ glass exhibited the memory effect. It is well known that B₂O₃ glass contains isolated structural units, called boroxols,⁴⁷ in contrast to the three-dimensional network of SiO₂ glass. Thus, the boroxol structure may behave like a region with different properties. In this sense, the single component B₂O₃ glass is considered to contain “concentration fluctuations.”

2. Low loss optical fibers

For optical fibers for communication, a high transparency, i.e., ultra-low optical absorption at the relevant wavelength(s) is an essential quality. *For commercial high purity silica glass fibers, scattering loss, which is caused by density fluctuations, becomes a limiting factor of high transparency.* One way to improve the optical transmittance characteristics of the optical fibers is thus by reducing density fluctuation of glasses. Since the density fluctuation is proportional to the fictive temperature of the glass, one can reduce the fictive temperature of silica glass to obtain lower-loss silica optical fibers. A silica glass fiber of 125 μm in diameter drawn at high temperature has a fictive temperature of approximately 1650 °C.^{48,49} A lower-loss optical fiber can be produced by passing a freshly drawn fiber through a furnace held at a temperature lower than the fictive temperature of the freshly drawn silica glass fiber. Saito *et al.*⁵⁰ showed that by this method, a silica glass optical fiber with a lower fictive temperature, and consequently, a lower loss can be produced. They showed that the fictive temperature can be reduced by several hundred K by this method. This corresponds to approximately 40% reduction of the optical loss.

3. High loss glasses

A similar expression to Eq. (8) exists for mechanical and dielectric relaxation strength.^{28,51} At the critical point of immiscibility and the spinodal line, where the second derivative of Gibbs free energy becomes zero, the relaxation strength and the relaxation loss become infinity. At this point, all of the mechanical or electrical energy is converted to heat. Of course, this feature is not limited to oxide glasses but can be observed in other materials such as metals and polymeric materials.

C. Measurement of fluctuations and short and medium range order

As indicated in Sec. III A, both x-ray small angle scattering intensity extrapolated to zero angle and light scattering intensity at 90° can be used to measure the relative magnitude of density and composition fluctuations in glasses. X-ray small angle scattering has been used traditionally to

measure the size of submicron-scale dispersed phase in various materials including glasses. The most prevalent equation used in x-ray small angle scattering is Guninier's law⁵² given by

$$I(h) = I(0) \exp(-h^2 R_g^2 / 3), \quad (9)$$

which applies to a system with small particles of dilute concentration in a matrix. In this equation, h is a wavenumber with the magnitude of $(4\pi/\lambda) \sin(\theta/2)$, where λ is the wavelength of x-ray, 2θ is the scattering angle, and R_g is the radius of gyration. For small angle, since $\sin(\theta) \approx \theta$, the magnitude of $h \approx 4\pi\theta/\lambda$. Equation (9) is frequently used to determine the size of the dispersed particles since spherical particle with the radius, R_0 , is related to the radius of gyration by $R_g = (3/5)^{1/2} R_0$. The second phase particle size can be determined by plotting the logarithm of the scattered intensity as a function of the square of the wavenumber, h^2 , and evaluating the slope of the plot. For many homogeneous glasses, the small angle scattering intensity is constant, independent of the scattering angle. Some glasses, such as SiO₂ glasses, have a low angle broad diffraction peak, with its tail extending to small angle scattering angle, and the small angle scattered intensity decreases with decreasing scattering angle. Therefore, in order to eliminate the influence of the diffraction peak, the small angle scattered intensity extrapolated to zero angle, $I(0)$, is used often as a measure of fluctuation in glasses. In many cases, e.g., evaluating the change of density fluctuation of a glass with fictive temperature, relative magnitude of zero angle scattered intensity is sufficient. The zero angle small angle scattering intensity obtained by an extrapolation, in absolute units, is given⁵² by

$$I(0) = I_e (\Delta \rho_e)^2 N V^2, \quad (10)$$

where I_e is the scattered intensity by an electron, $\Delta \rho_e = \rho_e - \rho_{e0}$ is the deviation of the electron density, ρ_e , from the average electron density, ρ_{e0} , N is the number of the “particles” and V is the volume of the “particle.” The “particle” can be considered to be a unit of fluctuation. Since electron density is proportional to density of materials, the small angle scattered intensity can be used as a measure of density fluctuation, given by Eq. (7).

Since most oxide glasses are transparent, Rayleigh light scattering at intensity at 90° has also been used successfully to measure the density fluctuation.³⁶ Both x-ray zero angle scattered intensity and Rayleigh scattered intensity have been used to measure the concentration fluctuation also for a simple glass system such as binary glasses. For example, both scattered intensities have been used to evaluate composition fluctuation as a function of small additive component such as fluorine or chlorine to SiO₂ glass, since pure SiO₂ glass has no composition fluctuation.^{35,36}

There is one advantage of light scattering over x-ray small angle scattering in evaluating the fluctuation of glasses. When one can obtain Brillouin scattering intensity, I_B , (Longitudinal mode) together with Rayleigh scattering intensity, I_R , using same sample under identical experimental condition as shown schematically in Fig. 7³² their ratio,

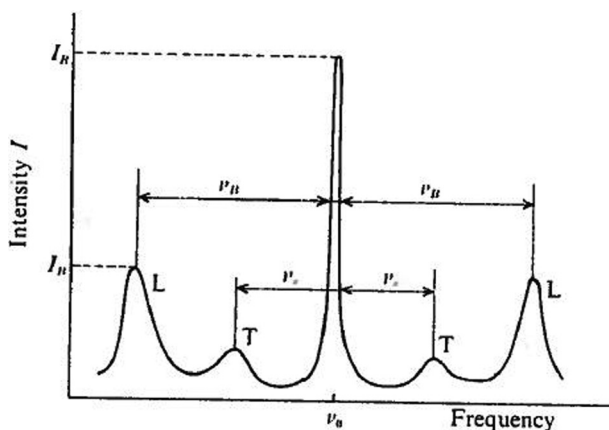


FIG. 7. Schematic diagram of Rayleigh scattering (center) and Brillouin scattering (L: longitudinal; T: transverse). Reproduced with permission from J. Zarzycki, *Glasses and the vitreous state*, translated by W. D. Scott and C. Massart (Cambridge University Press, 1982). Copyright 1982 Cambridge University Press.

$I_R/2I_B$, called the Landau-Placzek ratio, R_{LP} ,^{53,54} gives a direct measure of the sum of density fluctuation and composition fluctuation. Since the density fluctuation part can be calculated from the fictive temperature and compressibility of glass sample, composition fluctuation can be obtained as the balance. An example of such a measurement is shown in Fig. 8 for $\text{SiO}_2\text{-K}_2\text{O}$ system glasses.⁵⁴ The observed largest value of R_{LP} ratio at $\sim 10\%$ $\text{K}_2\text{O}\text{-SiO}_2$ glass coincides with the estimated critical composition for the immiscibility boundary of this binary glass system.

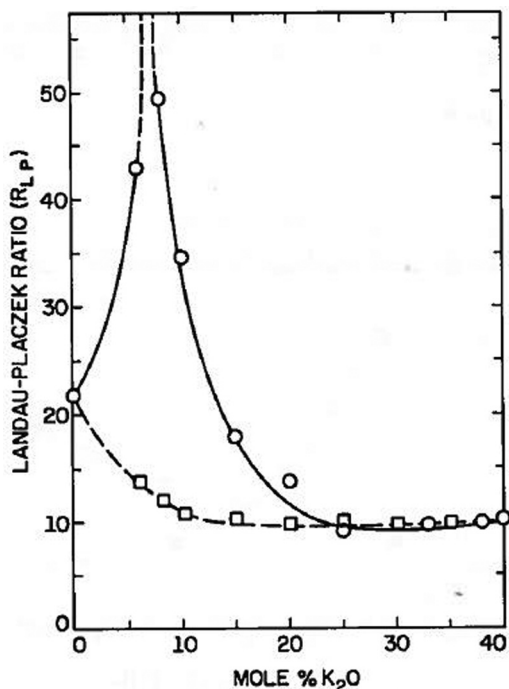


FIG. 8. Landau-Placzek Ratio of $\text{SiO}_2\text{-K}_2\text{O}$ glass. Square: density fluctuation; circle above square: composition fluctuation. Reproduced with permission from J. Schroeder, "Light scattering of glass," in *Treatise on Materials Science and Technology* (Academic Press, 1977), Vol. 12. Copyright 1977 Academic Press.

The scattering techniques described above allow determination of the structure factor, $S(k)$, or via the Fourier transform, the pair distribution function, $g(r)$. These quantities are averaged over the macroscopic volume; thus, intrinsically $S(k)$ and $g(r)$ are not very sensitive to fluctuations. Furthermore, they are dominated by the features associated with short-range order, such as atomic coordination, or distance between atoms. The tails of the structure factor can provide some information on the fluctuations (e.g., density fluctuations) but only on length scales ≥ 100 nm. Consequently, bulk scattering techniques are largely "blind" when the fluctuation length scale is in range of one to several tens of nanometers. However, some success in determination of compositional fluctuations was obtained via small angle X-ray (SAXS) studies of glasses.⁵⁵ In particular, it was concluded that some compositional inhomogeneities in metallic glasses occur on 1–100 nm scales, with their exact nature still subject to speculation.

To address this "blind" spot, Treacy and Gibson⁵⁶ have developed a technique called fluctuation electron microscopy (FM), with the original motivation to provide more information about medium range order (MRO) in amorphous materials. FM is the statistical analysis of fluctuations in diffraction from nanometer-scale volumes. Such local diffraction can be measured using a transmission electron microscope (TEM) and also, more recently, in X-Ray scattering.⁵⁷ FM reveals information based on higher order atomic distribution functions, which are more sensitive to medium-range structure than $g(r)$. In particular, FM studies of amorphous materials demonstrated the presence of medium range order (MRO)⁵⁸ which is not exhibited by computer-generated continuum random network (CRN) models of those materials.^{59–62} Instead, the structures were better represented by so-called paracrystalline (PC) models which consists of very small, 1–2 nm structurally ordered and strained grains in a CRN matrix.⁶³ This strain, potentially combined with a relatively small grain volume fraction, renders the structure indistinguishable from a CRN by diffraction.

While FM has been demonstrated to be very useful in exposing incipient and fluctuating structural order on a nanometer length scale, it might be also applicable to other fluctuations, such as density or composition fluctuations thus "filling the gap" in characterization of fluctuations over all relevant length scales. For example, a more recent focus of FM was on the investigation of multi-component bulk metallic glasses (BMG) where both structural⁶⁴ and compositional heterogeneities⁶⁵ were characterized. The characterization of density fluctuations by FM can be also envisioned for crystalline alloys. While for glasses, the reference structure with minimal fluctuations was the CRN, in the case of crystalline alloys one possible reference system is the fully ordered alloy that by definition has no fluctuations. Another possible reference system is a completely random alloy in which there are fluctuations but no spatial correlations.

The central idea of FM is to study the statistics of the image intensity. The simplest statistic is the average intensity. The average intensity is simply connected to $S(k)$, so it has little information about MRO. One more complicated statistic is the variance, or the normalized second moment V , defined as

$$V(K, Q) = \frac{\langle I^2(\mathbf{r}, k, Q) \rangle - \langle I(\mathbf{r}, k, Q) \rangle^2}{\langle I(\mathbf{r}, k, Q) \rangle^2} = \frac{\langle I^2(\mathbf{r}, k, Q) \rangle}{\langle I(\mathbf{r}, k, Q) \rangle^2} - 1, \quad (11)$$

where $I(\mathbf{r}, \mathbf{k}, Q)$ is the image intensity at point \mathbf{r} , \mathbf{k} is the scattering wave vector, Q is the objective aperture size, which controls the microscope spatial resolution, and $\langle \rangle$ indicates averaging over \mathbf{r} .

For a thin TEM specimen consisting of a single element imaged at moderate real space resolution ($\sim 10\text{--}20\text{ \AA}$), the kinematic coherent dark field image intensity, $I(\mathbf{r}, \mathbf{k}, Q)$ is proportional to⁶⁶

$$I(\mathbf{r}, \mathbf{k}, Q) \propto \sum_i \sum_j A_i(\mathbf{r}) A_j(\mathbf{r}) \exp(-2\pi \mathbf{k} \cdot \mathbf{r}_{ij}), \quad (12)$$

where \mathbf{r}_{ij} is the vector separating atom i from atom j , and the sums run over all the atoms in the sample. $A_j(\mathbf{r})$ is the point-spread function of the microscope, centered about the position of atom j . $A_j(\mathbf{r})$ is determined by the size and shape of the microscope objective aperture and the objective lens aberrations. For the simplest case of a circular aperture of radius Q and negligible lens aberrations, $A_j(\mathbf{r})$ is the Airy function. If, instead of using plane wave illumination, hollow cone illumination is used by averaging over all the in-plane directions of the scattering vector, the image intensity becomes

$$I(\mathbf{r}, \mathbf{k}, Q) \propto \sum_j \sum_i A(2\pi Q |\mathbf{r} - \mathbf{r}_j|) A(2\pi Q |\mathbf{r} - \mathbf{r}_i|) \times J_0(2\pi k |\mathbf{r}_j - \mathbf{r}_i|), \quad (13)$$

where $k = |\mathbf{k}|$ and J_0 is the zeroth order Bessel function. A detailed derivation of all the imaging equations in consistent notation may be found in Ref. 66.

Equation (11) provides an insight into the interpretation of the image intensity as a Fourier transform of a *local* pair distribution function $g_L(r', \mathbf{r}, Q)$ weighted by the Airy function. $G_L(r', \mathbf{r}, Q)$ is defined as

$$g_L(r', \mathbf{r}, Q) = \sum_j \sum_i A(2\pi Q |\mathbf{r} - \mathbf{r}_j|) A(2\pi Q |\mathbf{r} - \mathbf{r}_i|) \times \delta(|\mathbf{r}_i - \mathbf{r}_j| - r'), \quad (14)$$

where $\delta(r)$ is the Dirac δ -function. In bulk diffraction, a distribution function like $g(r)$ is an average quantity of the entire sample. Here, contributions to $g_L(r', \mathbf{r}, Q)$ come only from a small volume centered at point \mathbf{r} of the size proportional to $1/Q$. If we used a step function⁶⁷ instead of an Airy function for the weight, $g_{2A}(r', \mathbf{r}, Q)$ would be exactly a pair distribution function for the cylinder centered at point \mathbf{r} and extending through the thickness of the sample. Formulating the image intensity in terms of $g_L(r', \mathbf{r}, Q)$ highlights the essence of the FM. Each image point represents structural and compositional information of a small volume; thus, possible fluctuations are not averaged out over the macroscopic volumes.

An illustration of the sensitivity of the fluctuations to MRO is shown in Fig. 9 by $V(k)$ for CRN and three models

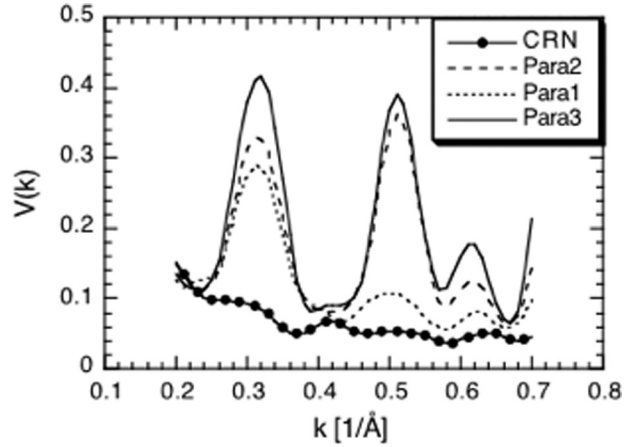


FIG. 9. $V(k)$, the standard fluctuation electron microscopy signal, calculated at $Q = 0.056\text{ \AA}^{-1}$ for of CRN and structures with $\sim 1\text{ nm}$ ordered domains. Reproduced with permission from Dash *et al.*, J. Phys. Condens. Matter **15**, S2425 (2003). Copyright 2003 Institute of Physics.

containing nm-scale ordered regions (with increasing size of the crystalline regions labeled Para 1–3) in an amorphous matrix. Clearly, $V(k)$ for the CRN is distinctly different for that of other structures. The structure factor $S(k)$ of the models (not shown) displays only small differences for all structures.

To determine the characteristic length scale of the fluctuations, one can examine the spatial correlations in the image intensity using the normalized autocorrelation function, $c(\mathbf{r})$, defined as⁶⁸

$$c(\mathbf{r}) = \frac{\langle [I(\mathbf{r}_1, k, Q) - \langle I(k, Q) \rangle][I(\mathbf{r}_1 + \mathbf{r}, k, Q) - \langle I(k, Q) \rangle] \rangle}{\langle [I(\mathbf{r}_1, k, Q) - \langle I(k, Q) \rangle] \rangle^2}, \quad (15)$$

where $\langle \rangle$ indicates averaging over \mathbf{r}_1 . Further azimuthal averaging can also be performed to yield a one-dimensional $c(r)$, where $r = |\mathbf{r}|$. $c(r)$ is normalized to one at $r = 0$ and goes to zero at large r .

In Fig. 10, $c(r)$ are shown for the CRN and 3 paracrystalline model structures with $Q = 0.056\text{ \AA}^{-1}$ and $k = 0.56\text{ \AA}^{-1}$.

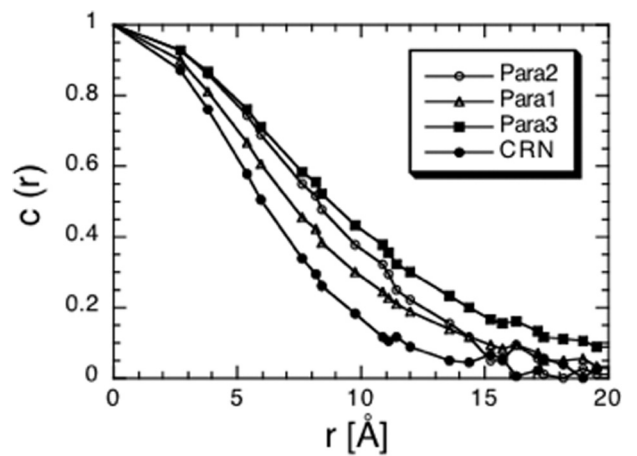


FIG. 10. The intensity autocorrelation functions, $c(r)$ calculated for the simulated images of the four model structures. $Q = 0.056\text{ \AA}^{-1}$ and $k = 0.56\text{ \AA}^{-1}$. Reproduced with permission from Dash *et al.*, J. Phys. Condens. Matter **15**, S2425 (2003). Copyright 2003 Institute of Physics.

In all cases, $c(r=0) = 1$, and $c(r)$ decays to zero for large r . However, the decay rate is fastest for the CRN and decreases with increasing MRO. From the rate of decay, one can extract the characteristic correlation length. In fact, the selection of the resolution, Q , can be used to probe specific length scales. The fluctuations over small length scale (less than $\sim 1/Q$) will be averaged out, while the dominant fluctuations over larger length scale (more than $\sim 1/Q$) will be exposed.

IV. STRUCTURAL AND COMPOSITION FLUCTUATIONS: ENGINEERED

As described in Sec. I, fluctuations in composition, density, and structure may be engineered, for example, through modulated thin film growth, through local manipulation with ion beams, or through controlled phase decomposition, such as in block copolymers. The example we focus on in this section is the control of engineered composite structures and how order parameters and correlation lengths in such materials may be used to tune both local and macroscopic properties.

A. Composite materials

Composite materials are widely used in engineering for their properties emerging from the interaction of the constituent phases. Typical engineering composites are composed from two or multiple phases, of which one plays the role of matrix. The other constituents are dispersed in the matrix and perform various functional roles, such as that of structural reinforcement or preferential sites of interaction with an external electromagnetic field. These “inclusions” may have various aspect ratios ranging from fibers to spheroids and may be distributed randomly or in a periodic way. Another class of composites has multilayered structure, with the layers being structurally and chemically different. Yet another way to classify composites from the structural point of view is to distinguish between structures in which phases are co-continuous (all phases percolate the domain occupied by the composite) and those in which one phase percolates and the others are isolated within this percolating phase (inclusions in a matrix).

In these materials, stochasticity is of a structural nature. The stochastic microstructure leads to stochastic stress and strain fields. Microstructural variability is either introduced intentionally or is unintentional. An example from the first category is that of polymers reinforced with fragments of glass fibers or with particles. Most composites with periodic structure fall in the second category and in this case structural variability is introduced by imperfect synthesis and manufacturing (see Sec. VII). In either case, the mechanical behavior is significantly influenced by the composition and the associated field fluctuations.

Formulating the discussion in this section in the language of Sec. II, for a composite with random microstructure, stochasticity is introduced via the parameters of the forward operator. The composite body defines the problem domain, V , and the distribution of material properties, $C(x, \xi)$, over this domain is affected by variability. This is represented by the presence of the random variable ξ in C .

Let us consider an elasto-static problem defined over the domain V of the composite. The system of interest here is closed. Material stochasticity appears in the mathematical formulation via $C(x, \xi)$, which enters the conservation of linear momentum equation. For this static problem, the equation reads $\text{div}(C(x, \xi) : \text{grad}(\mathbf{u}(x, \xi))) = \mathbf{0}$, where it was made explicit that the solution, $\mathbf{u}(x, \xi)$, is also a random vector field. The forward operator is deterministic in this case. The boundary condition can be either deterministic or stochastic. Stochastic boundary conditions add a second set of stochastic variables to the problem. In order to maintain simplicity and clarity of the discussion, we will focus here on deterministic boundary conditions.

The quantities of interest (QoI) in this type of problems are either of global type, i.e., quantities relevant for the overall mechanical behavior of the composite, or of local type, such as maxima of stress and/or strain fields. Global QoI are important in most applications as these represent the effective mechanical behavior of the material. Local QoI are important, for example, in damage initiation and fatigue. In both cases, the knowledge of the stochastic field $\mathbf{u}(x, \xi)$ is sufficient to evaluate the relevant QoI.

In practical problems, it is usually sought to solve only the forward problem in which the uncertainty in the structure propagates into the QoI. For composites, this implies that one may be interested in the variability of mechanical properties from sample to sample in a finite batch of parts. The forward propagation of uncertainty has been discussed extensively in the composite homogenization literature [e.g., Refs. 69–71]. In static mechanics problems, the momentum conservation equation is elliptic. This type of equation leads to a solution field, the displacement field $\mathbf{u}(x, \xi)$ in this case, which is smoother in the interior of the domain than at the boundary. A well-known embodiment of this behavior is the St-Venant principle in mechanics. If the QoI is global and expressed as an average over the problem domain, additional reduction of variability is introduced by the averaging operation.

It is also important to determine how optimization can be performed in this context. Once a global QoI is defined, and for given V and deterministic boundary conditions, one may perform an optimization of the QoI by varying the parameters of the random input field, $C(x, \xi)$. In principle, these parameters describe the probability distribution function of the values of C , and the spatial correlations of this field. In practice, one may take a more empirical route and describe $C(x, \xi)$ by introducing a set of measures of the distribution of inclusions. For example, in the case of a polymer filled with glass fibers, the fiber orientation distribution function, the number density of fibers, and their spatial correlations may be considered as proxies for $C(x, \xi)$. In a particle-filled composite, the random variables may be the positions of particles, their size, and possibly their material properties, if multiple particle types are used.

To demonstrate these concepts, we consider the specific example of a two-dimensional composite having a matrix with linear elastic properties and inclusions with viscoelastic properties.⁶ All inclusions are made from the same material and have the same size. The elastic constants of the

two phases are deterministic and known. However, the position of inclusions in the problem domain is stochastic. Therefore, the probability distribution function of \mathbf{C} , $p(\mathbf{C})$ is composed from two delta functions corresponding to the values of the material properties of the two phases. We consider for simplicity that all components of tensor \mathbf{C} have the same distribution function. The mean of this field is proportional to the filler volume fraction.

In this context, an optimization problem can be defined relative to a global QoI, for example, the composite stiffness, over all possible arrangements of fillers in the problem domain. In principle, this is a problem with large dimensionality. However, it is possible to reformulate it in terms of a small number of parameters, such as the multipoint correlation functions. The first order term in this set is the usual pair correlation function. If only this term is retained, the optimization problem is rephrased as ‘find the spatial correlation of filler positions that optimizes the composite “stiffness”’.

An answer to this problem is provided in Fig. 11. The figure shows the effective modulus of the composite, E_e , normalized by the modulus of the matrix, E_1 , function of the filler volume fraction, f . The fillers are considered linear elastic with stiffness 6 times larger than that of the matrix, $E_2=6E_1$. The data points represent results for various types of spatial correlations. The open circles and the continuous line correspond to the random distribution of fillers, i.e., in which the correlation function is a delta function and the correlation length vanishes. The filled circles correspond to an exponential correlation function. All other symbols represent microstructures in which filler positions are power law correlated

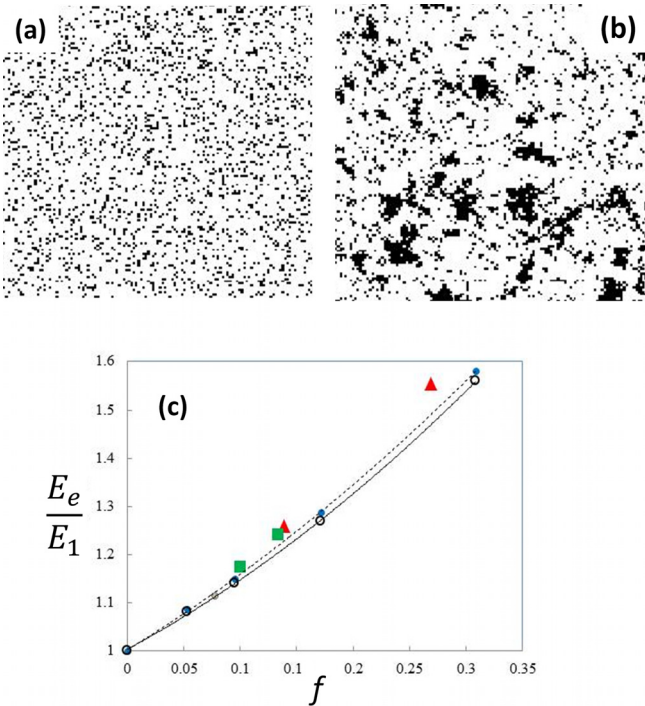


FIG. 11. Realizations of a 2D particulate composite with (a) random and (b) exponentially correlated distribution of inclusions, and (c) the variation of the effective elastic modulus of the composite with the filler volume fraction for random filler spatial distributions (open circles and continuous line), filler distributions with exponential (filled circles and dashed line), and power function correlations (other filled symbols).

and hence the composite has a fractal microstructure. Fractal structures having various fractal dimensions are considered. Power law correlations do not have a characteristic correlation length (i.e., are scale free); however, the fractal dimension indicates how fast the correlation decays. It is observed that spatial correlations have a non-negligible effect on the effective modulus. The dominant effect is due to the volume fraction, but the effective modulus may be increased by up to about 10% by filler clustering. In other words, increasing the correlation range has a stiffening effect.

A similar effect introduced by spatial correlations of particle positions (particle clustering) occurs with respect to the effective damping coefficient. If one assumes that dissipation takes place only in inclusions (i.e., the matrix is purely elastic), it can be shown that the effective dissipation of the composite increases sharply with increasing the range of spatial correlations of inclusion positions at given filler volume fraction.

Figure 12 shows the effect of the correlation length on a norm-type QoI—the maximum principal stress in the matrix. This local parameter is important for damage nucleation. The figure shows the probability distribution function of the maximum principal stress resulting from an imposed far field (deterministic) uniaxial deformation. The open circles correspond to the random distribution of fillers (delta function correlation), while the filled symbols correspond to the fractal distribution (power function correlation). Both distributions are normalized by their mean. It is observed that the distribution for randomly distributed fillers is shifted to the right, indicating higher probability of damage nucleation in these composites.

Another informative example is that of a composite with randomly distributed inclusions and in which inclusion properties vary from inclusion to inclusion.⁷² Consider a case in which the matrix is homogeneous and of modulus E_1 , while the Young’s modulus of inclusions is sampled from a distribution function of mean $E_2 = 6 E_1$ and of coefficient of variance λ . One is interested in the effect of λ , at constant E_2 , on the overall composite modulus, E_e . Figure 13 shows results for two filler volume fractions, f . The normalized mean composite modulus, E_e/E_1 , is re-normalized with the respective

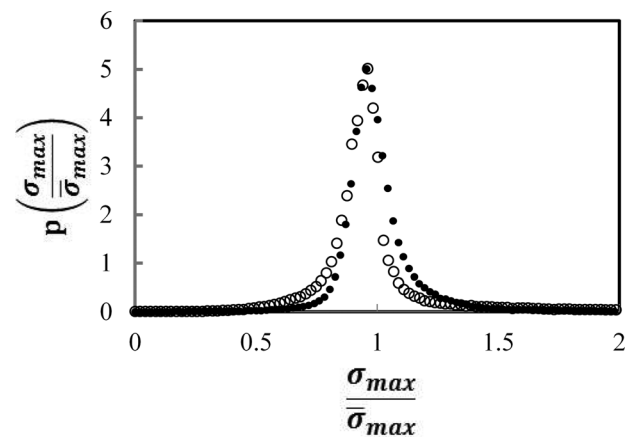


FIG. 12. Probability distribution functions of the maximum principal stress in a composite with random filler distributions (open circles) and power function correlation of the filler spatial distribution (filled circles). The variable is normalized by its mean in both cases.

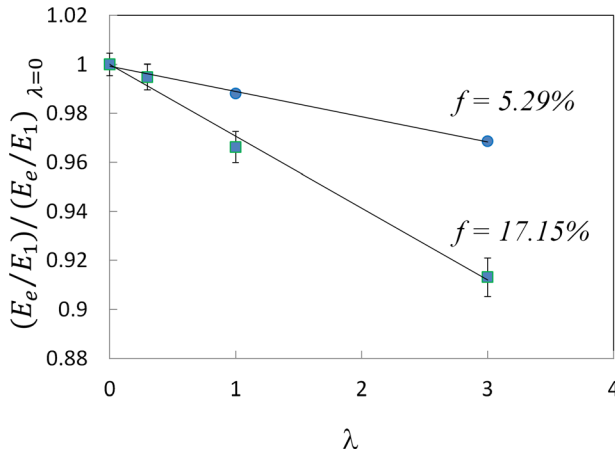


FIG. 13. Normalized composite modulus versus the coefficient of variance of the distribution function of inclusion moduli, at constant mean of the same distribution function, for two filler volume fractions, f . Increasing the variability of filler moduli leads to overall composite softening.

quantity corresponding to the case in which all inclusions are identical, i.e., all have modulus $E_2 = 6 E_1$ and $\lambda = 0$. The figure shows that as the variance of the distribution function of filler moduli increases, the mean composite modulus decreases, which is not necessarily an expected behavior.

A similar effect was reported for a network of cross-linked elastic filaments distributed randomly in space and in which each filament is made from a material of elastic modulus sampled from a distribution.⁷³ The overall elastic modulus of the network decreases with increasing the variability of fiber material properties. Likewise, Dimas *et al.*⁷⁴ observed the same effect in stochastic composites.

The thermal conductivity of composites containing inclusions of same properties and various dimensions (filler size polydispersity) exhibits an opposite trend.⁷⁵ As the volume fraction of inclusions, the mean inclusion size, the thermal conductivity of inclusions, and of the matrix are kept constant, but the inclusion size is sampled from a distribution function of increasing variance, the thermal conductivity of the composite increases.

In polymer-based nanocomposites, it is generally thought that optimal properties result when the nanofillers are randomly distributed in the matrix, with agglomeration kept to a minimum. This concept is rooted in the observation that inorganic fillers produce an interphase of matrix material around them. The physical properties of this interphase are different from those of the matrix, although the chemistry is identical to that of the matrix. Interesting composite-scale properties emerge when the interphases surrounding fillers percolate and their contribution becomes measurable on the global scale. Given the very large surface area of nanofillers, the interphase volume is much larger in nanocomposites than in microcomposites of same constituents and filling fraction. Therefore, interphase percolation happens at very small filler volume fractions in nanocomposites.

Due to the practical difficulties associated with manufacturing a nanocomposite with prescribed filler spatial distribution, optimal properties are associated with the random distribution of fillers, i.e., the most dispersed

distribution possible. On the other hand, many mechanical and dielectric properties are actually worse than those of the unfilled matrix if large clusters of nanoparticles are produced during manufacturing. A broad range of microstructures exists between these two extremes and the opportunities provided by controlling the spatial distribution of fillers have not been fully explored to date.⁷⁶

An example of a natural composite material structured on multiple scales is bone. The constituents of bone are mineral (hydroxyapatite) and proteins. As in shells and insect armor, small mineral platelets are separated by layers of organic material of nanoscale thickness. The dense mineral distribution provides high modulus and strength, while the organic inter-layers produce sufficient local strain accommodation to mitigate stress concentrations and allow crack deflection when mineral plates fracture. The toughness of such composites is remarkable.

The bone structure has several important scales (Fig. 14). Osteons are the dominant feature on the 100–200 μm scale. These are composed from lamellae of several microns thickness arranged in a concentric fashion. Each lamella is made from a large number of fibrils packed together much like a coaxial cable. The fibrils are made from mineral platelets and protein interlayers and have submicron diameters.

The stiffness, strength, and toughness of bone are controlled by this multiscale structure in ways that are not entirely understood at present. Geometric variability as well as some degree of variability in constituent properties exists on all scales, from that of the mineral platelets to the osteons. Elucidating the effect of these fluctuations on the macroscopic mechanical behavior of bone is a fascinating frontier in materials stochasticity.

V. KINETIC FLUCTUATIONS

In this section, we focus on the class of stochastic origins #3 in the Introduction, which arise from kinetic fluctuations. By kinetic fluctuations, we mean stochastic variations in structure that have their origins from a distribution of events or processes in time, for example, nucleation phenomena, phase transformations, and crystallization. According to the definition introduced in Sec. I, these stochastic processes are generally *inherent*, but can be *engineered* to control microstructure (and thus properties and performance) through judicious control of processing conditions.

A. Nucleation phenomena

Nucleation is associated with the early stages of the creation of a new state or defect in a material that was not previously present. Nucleation phenomena are highly sensitive to the local material state, and inherent variability in the material at the micro and atomic scales leads to a high degree of variability in the nucleation phenomena. Furthermore, the stochastic nature of the nucleation phenomena has a large impact on subsequent growth processes. In fact, in many cases, the variability in the nucleation process is much higher than that associated with growth, and thus, the stochasticity of the final micro-structural state is primarily dictated by the stochasticity of nucleation. The nucleation process often has

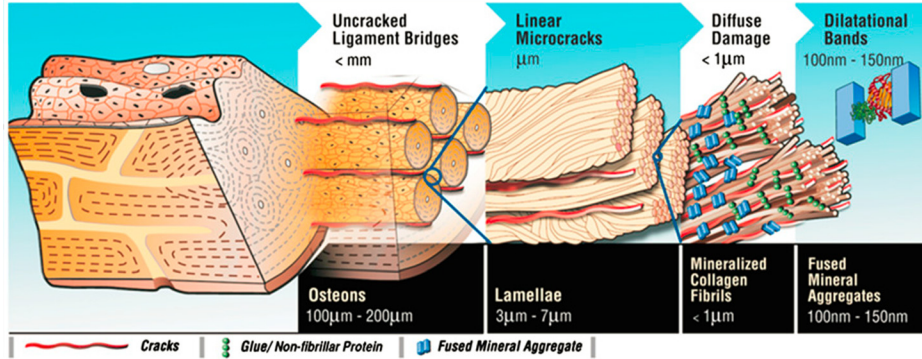


FIG. 14. Schematic representation of the hierarchical microstructure of bone. Reproduced with permission from Poundarik *et al.*, Proc. Nat. Acad. Sci. U. S. A. **109**, 19178 (2012). Copyright 2012 National Academy of Sciences.⁷⁷

a higher degree of variability than growth processes because nucleation is generally more susceptible to finer scale fluctuations. Examples of nucleation processes demonstrating this are described later in this section. Understanding and modeling the stochasticity of nucleation phenomena are essential to accurately capturing the stochasticity of many material microstructures and their behavior.

Considering the framework laid out in Sec. II, nucleation phenomena can be thought of as both relating to a *stochastic QoI* resulting from a prior stochastic physical process as well as imparting stochasticity to the *initial data* for subsequent *forward propagator* growth processes leading to a final state. Figure 15 illustrates this, where a representative microstructure, defined in terms of stochastic parameters ξ leading to a distribution of material properties over the microstructure $D(x, \xi)$, is subjected to a load f , for example, mechanical or thermal, defined in terms of stochastic parameters ζ_0 . The material response to that loading is defined through a forward operator \mathfrak{F} , which results in a distribution of driving energy E_d for nucleation events. Furthermore, there is an energy barrier to nucleation, E_b , which has some variability associated with variability in the micro- and nano-scale structure. Nucleation is the rare event that occurs when the driving energy E_d exceeds the energy barrier E_b (the overlap of the tails of the distributions in Fig. 15) resulting in the formation of a distribution of nuclei. The *QoI* is then related to the random variable defined by $\zeta_1 = (E_d - E_b)$, and the probability of nucleation is the probability of ζ_1 being greater than zero ($P\{\zeta_1 > 0\}$). Thus, the highly stochastic nature of nucleation is associated with the large variability in the driving energy and in the energy barrier due to both microstructure variability and atomic scale variability, which we are unable to measure accurately at all locations in the material. That distribution of nuclei also serves as the initial conditions (denoted $I.C.(\zeta_1)$) for ensuing growth processes.

Specific examples of nucleation that exemplify this formalism include deformation twinning, phase transformation, recrystallization, and fatigue cracking.

1. Example 1: Deformation twinning

A deformation twin nucleates through a stress-driven transformation of grain boundary dislocations that dissociate into a stable twin nucleus.⁷⁸ The nucleation of a twin is an atomic scale process with multiple potential pathways, which depend on a range of micro and atomic scale material features, such as grain orientation, grain boundary character, dislocation structures, etc., as well as the local stress state.⁷⁹ As such, at the grain scale without knowledge of the finer scale details, twin nucleation appears to be highly stochastic. For example, Beyerlein *et al.*⁸⁰ observed a large degree of variability in twin nucleation in Mg, with a significant fraction of grains poorly oriented for twinning, i.e., with a low resolved shear stress in the twin system, developing twins, and likewise, a significant fraction of grains favorably oriented for twinning not developing twins. On the other hand, the subsequent growth of deformation twins is observed to be relatively deterministic, with the rate of growth increasing with the resolved shear stress on the twin system.⁸¹ Thus, deformation twinning demonstrates how the stochasticity of nucleation dictates the stochasticity of the final state, as previously suggested.

In the context of the framework laid out in Secs. I and II, and illustrated for nucleation in Fig. 15, the stochastic process of deformation twin nucleation starts with a stochastic microstructure that is subjected to mechanical loads resulting in a deformed microstructure. The microstructure is polycrystalline and is characterized by a set of stochastic parameters ξ , such as grain size, shape, and orientation distributions. The mechanical loading may be a deformation or a stress, which may also be stochastic, defined in terms of

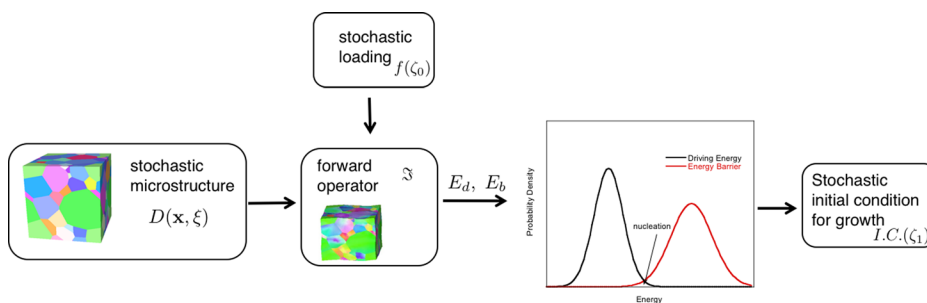


FIG. 15. Stochasticity of nucleation.

parameters ζ_0 . Due to the anisotropic mechanical behavior of the individual grains in the polycrystal, a complex distribution of stress and deformation results at the grain scale, which depends on ξ and ζ_0 . The driving energy for twin nucleation, E_d , is directly related to the resolved shear stress on the twin systems, and depends on the local stress state and grain orientation. The energy barrier for twin nucleation, E_b , can be related to a critical nucleation strength that depends on the local microstructural and atomic scale features, as described above, and is highly stochastic. Beyerlein and Tome⁸² define the critical nucleation strength distribution as a Weibull distribution. The probability of a twin nucleating at any location in a grain can then be defined as the probability that the maximum resolved shear stress on the twin system exceeds the critical nucleation strength. Once the twin nuclei are defined, that distribution of nuclei, represented by stochastic parameter ζ_1 , together with the resolved shear on the twin systems, may serve as the initial conditions for deformation twin growth leading to the final microstructure.⁸¹

2. Example 2: Nucleation of 2D materials during epitaxial growth

Nucleation of a new phase during growth is generally a stochastic process, as illustrated in Fig. 16 for a topological insulator Bi_2Se_3 . The stochastic nature of the nucleation is magnified here by the fact that Bi_2Se_3 is a layered material. As such, nucleation on a flat terrace becomes inevitable after the completion of the growth of a prior nucleated layer. The exception is when the growth is in a spiral mode which preserves the growth front.⁸³ Even in the latter case, there is still the issue of initiating the growth which will determine the morphology and structure of the film thereafter. To this end, one may argue that the growth may take place at step edges

of the substrate. However, for Bi_2Se_3 grown on Si for example, not only the structures do not match but also the steps of Si do not match the monolayer height of Bi_2Se_3 , either. (The Bi_2Se_3 step height is about 1 nm, where the Si single layer step height is 0.32 nm and double layer step height is 0.64 nm with one being more abundant than the other depending on the experimental conditions).⁸⁴

Here, for the sake of illustration, we consider only the simple case of nucleation of Bi_2Se_3 on a flat surface. Since Bi_2Se_3 is a layered material with weak van der Waals (vdW) binding between the layers and with the substrate, we do not have to specify the substrate in this discussion. With these simplifying assumptions, we can now define the problem as follows: during deposition of the relevant species/molecules, there will be many different small clusters both above and on the surface before they can agglomerate and nuclear into islands with a clearly-defined epitaxial relationship to the substrate. For molecular beam epitaxy (MBE) growth, these would be Bi_iSe_j clusters (where i and j are natural numbers) of their own respective energies—as it turns out, our first principles calculations (unpublished) show that some of the clusters are relatively low in energy but most of them are relatively high in energy. It is clear that those on the surface will have lower energies as long as they can spontaneously form some sort of chemical bonds with the surface without having to overcome significant reaction barriers.

To solve the problem which is a process of energy minimization through the agglomeration of clusters via cluster diffusion, we need to set up the boundary condition(s) that best matches experiment. In particular, we can say that at a given time t , there are a total of $N(t)$ clusters on the surface, namely,

$$N(t) = \sum_{i,j} n_{ij}(t), \quad (16)$$

where $n_{ij}(t)$ are the number of Bi_iSe_j clusters at the specified time. As the growth process proceeds, $N(t)$ will change due to deposition but also due to the growth, namely, the incorporation of the clusters into epitaxial films or into elemental bulk materials (as denoted in Fig. 16 as “nucleate Bi_2Se_3 ,” “nucleate bulk Bi,” and “nucleate bulk Se”). We assume that the clusters diffuse on the flat surface to find the step edges of nucleated Bi_2Se_3 , namely, the growth front, to be incorporated [i.e., dropped out from Eq. (16)]. Unless in extreme growth conditions such as highly Bi-rich or Se-rich, nucleation of their respective bulk phase can be ignored. Our primary concern, i.e., the clusters, is also tabulated in Fig. 16 in the order of their respective sizes. Generally speaking, clusters to the right would contain more Bi atoms than those to the left; clusters to the above would contain more Se atoms than those to the bottom.

As the clusters diffuse, some of them will bump into each other, giving rise to agglomeration, and some of them may disintegrate. However, the latter happens only if the original clusters are highly unstable when compared to the smaller ones they disintegrate into. The diffusion of the clusters may be described as undergoing a biased random walk in the phase space⁸⁵ depicted in Fig. 16, with entropy greatly

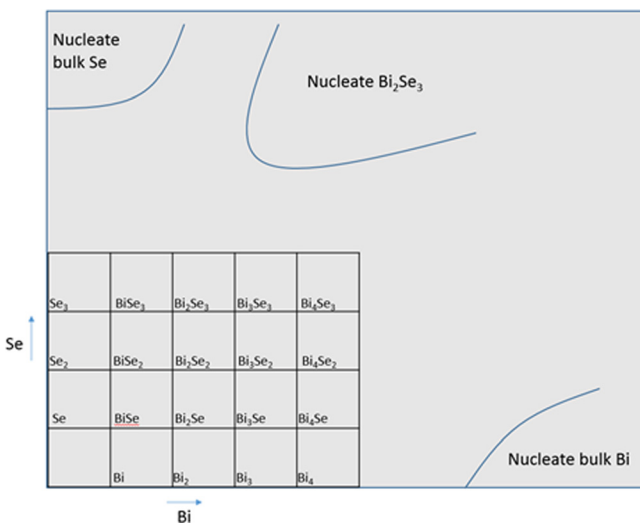


FIG. 16. A cluster phase space indicating connections between clusters of various sizes. Horizontal axis is the Bi content, whereas vertical axis is the Se content. In this space, each cluster has its own coordinates. A cluster can grow by taking a smaller or equal sized cluster(s) at its lower/left part in the figure to become a larger one located on its upper/right part. Through such a process, some of the clusters in the lower/right quadrant will eventually grow large enough to enter one of the nucleation regimes shown in the other three quadrants.

favoring small cluster sizes. The nucleation rate for the epitaxial growth is then determined by the number of random walkers per unit time which attain a radius R greater than the critical radius R_c for nucleation of an energetically stable cluster, or alternatively they enter the region in Fig. 16 demarking the nucleation of Bi_2Se_3 .

The scientific challenge to this problem is how to balance the Gibbs free energies of the various clusters, which contain both the internal energy of the clusters and the contribution from entropy at the growth temperature with the constraints of limited diffusion on the surface. As mentioned earlier, these clusters tend to stick on the surface by spontaneous formation of chemical bonds (presumably weaker than a typical chemical bond), despite the fact that the interface is vdW-type after the completion of the growth of the epilayer. This stickiness of the surface, or chemical bond formation, is the ultimate reason for the limited diffusion of the clusters on the surface.

Now comes the issue of stochasticity: what are the energies of the clusters when they enter the step edges of an already nucleated Bi_2Se_3 ? Clearly, there can be a large variation in these energies at any moment. In addition, in developing our physical picture above, we have made several assumptions to simplify the problem. Any factors that break these assumptions will appear as systematic errors, and any unforeseen events in a real physical system will appear as stochastic errors, against our simulated results. The beauty of the stochasticity concept is that it empowers us to develop a quantifiable solution to the problem that is bounded by scientifically-defined error margins. The stochasticity theories, such as those discussed in Sec. II of this review, provide the mathematical means, for us to assess the errors and to differentiate between them. To advance from Fig. 16 further, we therefore postulate the existence of a cluster-averaged Gibbs free energy per element. This average energy works the same way as the chemical potential μ in equilibrium theory,⁸⁶ except that it is subject to additional constraints not relevant to μ . Hence, we term the average energy as a cluster-averaged chemical potential, $\bar{\mu}$. In the current case, there are two such potentials, namely, $\bar{\mu}_{\text{Bi}}$ for Bi and $\bar{\mu}_{\text{Se}}$ for Se. Once $\bar{\mu}$'s are defined, the energies for cluster incorporation at the growth front also become deterministic. Therefore, we can apply standard first-principles approaches^{87,88} to quantitatively study the nucleation and growth processes during epitaxy and illuminate the underlying stochastic mechanisms.

3. Example 3: Recrystallization

Recrystallization results in a change in texture and grain structure in a deformed metal at elevated temperatures. The nucleation stage of this process plays a decisive role in defining the resulting texture and grain structure.⁸⁹ During recrystallization, new grains grow from certain subgrain cells formed during deformation that act as nuclei, and the new grains that are growing absorb other grains, which are shrinking. The orientation of a new grain is that of the cell from which it was formed. Only a very small fraction of cells formed during deformation become nucleation sites for new

grains.⁹⁰ However, it is not a completely random process. Certain factors affect the likelihood that a cell will become a nucleation site, such as the level and type of misorientation angle between the cell and its neighbors and the cell size.^{91,92} Considering Fig. 15 again, the stochastic microstructure would consist of a polycrystal characterized by the grain size, shape, and orientation distributions as well as a distribution of stored energy associated with dislocations resulting from prior deformation, which could be defined in terms of a set of parameters ξ . The loading, characterized by parameters ζ_0 , would be the temperature distribution. In this case, the driving energy, E_d , is the difference between the stored energy in the surrounding material and that in the cells, where cells will tend to grow if they have a lower stored energy than the surrounding material such that cell growth lowers the system energy. The energy barrier to cell growth, E_b , depends on the micro and atomic scale features of the subgrain boundary, including the level of misorientation, whether the misorientation is of a special type, local dislocation structure, etc., and thus, exhibits a high level of stochasticity. Once a distribution of nuclei has been formed, ζ_1 , subsequent grain growth occurs. The grain growth process is also stochastic, with the rate of grain growth depending on the local driving energy and grain boundary mobility. The driving energy is associated with the local grain boundary curvature and stored energy. The grain boundary mobility, which can be thought of as the inverse to the energy barrier for growth, is influenced by many of the same factors as for cell growth, but less influenced by the atomic scale feature, resulting in a lower level of stochasticity in grain growth as that in nucleation.

4. Example 4: Fatigue cracking

The fatigue life of a material, defined as the number of stress cycles to failure for a given loading history, is known to have a high degree of variability, frequently ranging over one or two orders of magnitude. The number of cycles to failure can be divided into two parts, the number of cycles to nucleate a fatigue crack, and the number of cycles to propagate the crack to failure. It is in the early stages of fatigue crack nucleation and growth when variability is greatest, and the microstructure plays a key role. Specifically, when the cracks are microstructurally small, i.e., smaller than the typical grain size, the variability in the local stress and strain field due to the local grain orientations and microstructural features, such as grain or twin boundaries, play a key role in both nucleating and arresting cracks. The importance of the early stages of fatigue crack nucleation on the fatigue life variability has been recognized, and efforts have been initiated to develop physically based probabilistic models to quantify the uncertainty in the remaining life using approaches similar to that outlined here.^{93–96} As the cracks grow, the effect of the microstructure is diminished, and once the cracks are passing through multiple grains, the crack propagation becomes more predictable (less stochastic), typically following a Paris Law⁹⁷ behavior remarkably well.

VI. FRUSTRATION AND DEGENERACY

The structure of matter begets the properties of matter. Arguments for preferred structures are energetic in nature and therefore thermodynamics can be brought to bear on the problem of determining the lowest energy structure. In many cases attainment of an “ideal” (i.e., lowest energy state) structure is possible provided enough degrees of freedom are present. For various reasons, be it bonding, magnetic ordering, or mesoscopic features of a system, the achievement of the ideal structure is in many cases impossible to realize, not due to kinetics or proximity to equilibrium, but because the ground state is inaccessible. This leads to the development of a frustration. The onset and kinetic evolution of the frustration in such a system are inherently stochastic.

The problem of frustration arises from the rationalization between the structural constraints of the system and the energy landscape defined by its thermodynamics. While kinetically frustrated systems can exist, e.g., in structurally amorphous materials, in thermodynamic equilibrium these systems are not precisely frustrated since fully crystallized or at least phase-separated structures remain attainable with a long enough timescale. In the present discussion, we will limit this treatment of frustrated systems to those systems that cannot attain a “symmetric” equilibrium, based on the incompatibility between the driving forces for minimizing the energy of a system and the constraints that enforce a particular structure under consideration.

One paradigmatic example of a frustrated system can be imagined to be three magnetic moments arranged at the vertices of an equilateral triangle [Figs. 17(a) and 17(b)]. In this system, there is no possible arrangement of the magnetic moments that will achieve an energy minimum in an anti-ferromagnetic configuration. Because neighboring magnetic moments tend to have mutually anti-parallel configurations, in this scenario, there are two high-energy configurations and six configurations that are equivalent in energy. The microstate of the system will be determined by external forces as there is no internal force that will drive the system to any one of these particular six states. In the absence of external force or energy added to the system, the realization of a specific configuration will be totally stochastic in nature, with a single realization among any of the degenerate microstates. This simple example suggests a common feature: frustration and degeneracy are intimately related. Frustration leads to degeneracy, which, in turn, imposes the use of probabilities to develop an interpretation of a given observation. We can also argue the reciprocity of this relationship since degeneracy can lead to frustration.

In another example related to carbon materials, the hybridization of one s orbital and two p orbitals of carbon results in many attractive properties that are consequences of the intrinsic rules of sp^2 hybridization. These rules impose that each carbon atom must be σ bonded to precisely three neighbors, exactly one of these necessarily possessing an additional π bond. This relatively simple idea of drawing organic structures in terms of two single and one double bonds per carbon is named after August Kekule, who proposed the concept in the 1800s.⁹⁸ The Kekule structure, as a

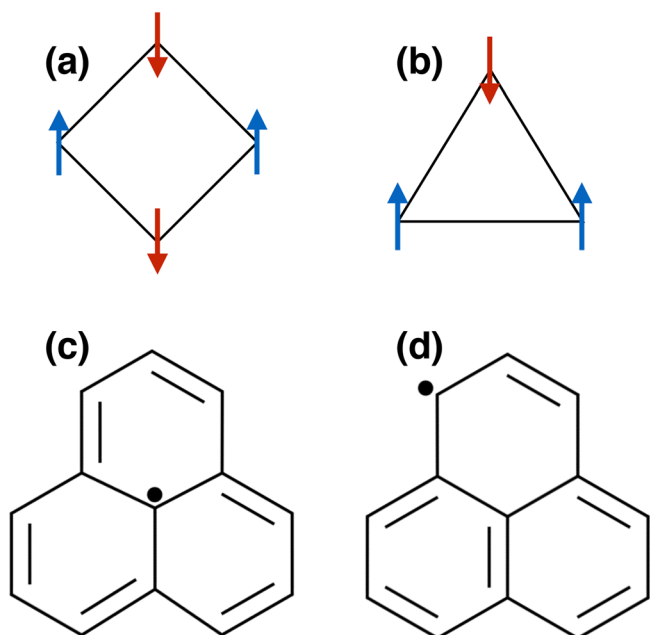


FIG. 17. Examples of frustrated systems: (a) and (b) Show spin configurations in antiferromagnetically interacting systems. (a) An optimal interaction is achievable on a square lattice but (b) is impossible in the frustrated system made up from a triangular system. It follows that the triangular arrangement displays a net magnetic moment. (c) and (d) Kekulé representations of the smallest carbon sp^2 -based triangulate system. The geometry of the structure makes it impossible to associate each carbon atom with exactly one double bond. The unmatched atom corresponds to an unbounded π orbital electron, or free radical, represented by a dot. It follows that the structure is non-Kekuléan and its ground state is a doublet spin state. This frustration is similar to the one observed on the spins located at the vertices of a equilateral triangle and results from the incompatibility between the molecule geometry and the requirements of 3 σ and one π bond per carbon atom.

model, became outdated with the development of quantum mechanics, which established a more complex picture where knowledge of the localization of an electron is expressed as a probability distribution. However, the original model remains a valuable concept and due to its inherent power as a metric for structural characterization, the Kekulé model can be used to highlight the emergence of topological frustrations and provide a better understanding of the high reactivity of small organic compounds. Topological frustration, when viewed by quantum mechanics with regards to sp^2 carbon, refers to open and localized π orbital shells leading to a non-singlet state having the lowest ground state energy. In the language of chemistry, a single frustration corresponds to a doublet due to the fact that a sp^2 carbon atom is unable to link to any double bond under any possible Kekulé structure (without creating additional unlinked atoms). In the context of graph theory, starting from a network made up of a structure’s adjacency matrix (i.e., a listing of all neighboring atoms), a frustration appears when the maximal matching of a graph leaves unmatched nodes. In addition, topologically frustrated structures have also been known as concealed structures and non-Kekuléan structures. An example of this same phenomenon viewed from different disciplines is illustrated in Figs. 17(c) and 17(d), using the smallest Triangular Zigzag Graphene Nanoflake as a demonstration structure.

Another example is that of a collection of polycrystalline grains. Glicksman⁹⁹ showed that under the standard assumptions of grain growth (i.e., fixed external dihedral angle) no polyhedral like grain (Glicksman's so-called N-hedra) with zero mean curvature can be constructed in three-dimensions. If the average curvature of an infinite ensemble of N-hedra is set to zero, then the average number of faces among the infinite set is $N \approx 13.39$. The implication of this energetic result is that real constructible polyhedra-like grains would have face curvatures that are either positive or negative and therefore imply growth or shrinking of the grain, Fig. 18. Because the granular nature of the system precludes it from ever attaining the optimal number of sides, there is a tug-of-war between the realization of configurations that tend to, yet will never achieve, the lowest energy state. Therefore, we see that it is the incompatibility between locally minimizing the energy due to the mean curvature of the interfaces and the structurally realizable physical system that leads to frustration: Grain growth in the present context is therefore frustrated and can never achieve the energy minimum expected from a coarse grain analysis.

In each of these three examples, stochasticity emerges from the impossibility to satisfy the constraints of the local interactions. It follows that the lowest attainable state is degenerate and the choice of any particular observed state is intrinsically probabilistic.

Of course, physical systems are quantized at the atomic scale. Many physical systems, however, can be treated as continuum under appropriate assumptions. In the case of quantum systems, an enumeration approach will elucidate the possibility of frustration through inspection of the energy states associated with different configurations. In some cases, there may be a large degeneracy that admits the possibility of structural frustration (although the system itself has no thermodynamic minimum). In other cases, there will be an extremum in energy that is only eliminated as a possibility when some structural symmetry is broken. These systems are not capable of geometric frustration until that symmetry breaking event (e.g., the discussion of the strained nanotube below).

In the case of continuum systems, the number of particles is typically so large that statistical mechanics becomes necessary. In these systems, we can treat the energy as a continuum quantity defined by the extensive quantities of the system. In this case, the energetics may admit a minimum and therefore it would appear upon first inspection that frustration is unlikely. However, it may be necessary to inspect states of energy near the extremum point for "energetic ripples" that would admit frustration. These states originate from the presence of shallow metastable local minima that have a finite population at room temperature. They are likely to not display the full symmetry of the structure that sustains them and frustration may ensue.

In other cases, we may have to define the continuous energetics of the system and then apply a "selection template" to the energy to define allowable and disallowable continuum states. It is not until we apply this template that we can directly observe the consequences of structural frustration on the system. For example, consider the discussion of polycrystalline structures above. The template in this case is

the allowable cell geometries combined with the continuum energies derived by assuming polycrystal ensemble averages.

Once we define the continuum energy landscape, we must then invoke structural constraints on the system. These structural constraints serve two purposes. First, they can help to break the symmetry of the system such that a frustrated system is structurally possible and second the constraints limit the system's ability to achieve a global minimum. This is another example of not being able to rationalize the energetic interactions and the structural configurations. If we fundamentally limit a structure from realizing its lowest energy, then it is possible (but not guaranteed) that a frustrated system will result, the reason being that the metastable configuration will not display the full symmetry of the structure and therefore may correspond to a frustrated distribution of the interactions within the system.

Consider the case of a strained carbon nanotube. Frequently observed elementary defects in carbon nanostructures range from bond rotation (or Stone-Thrower-Wales defects¹⁰⁰) where four hexagonal rings transform into two pentagons and two adjacent heptagons, i.e., a 5775 defect) to a dimer removal (a 585 defect) or dimer addition (a 7557 defect). In the event that a defect is introduced, we next consider where the defect should be located. In many of the possible defect sites, the resultant reduction in energy is equivalent. Consider the sites around the circumference of the nanotube at a fixed distance from the end of the nanotube. In every case, the introduction of the defect will result in an energy reduction for the system. Where then is the appropriate location for the defect to emerge? We assume that no *a priori* information is available to define the best location for a defect and instead consider that a random event will nucleate the defect somewhere along the length of the nanotube. This then represents the emergence of a frustrated system by a stochastic event. This event initiates a second stochastic property of the system defined by the degeneracy of the energy landscape. For example, the defect can migrate throughout the body of the nanotube (similar to a vacancy in a crystal) and create equivalent energetic structures. The system effectively explores the degeneracy defined by the thermodynamics of the nanotube structure (Fig. 19).

The examples shown in this section focused on the intricate relationship between structural frustration and degeneracy as the origin of stochasticity. In this particular case, it is the degree of degeneracy of the most stable configuration attainable under normal condition that leads to fluctuations in the observed state. The equivalent systems can evolve and diverge along an unlimited number of pathways, thereby creating stochasticity. Linking to the framework presented in Sec. II, the phenomena described here is the uncertainty in the initial data: in this case, this uncertainty is not related to lack of accuracy in experimental measurements but rather to the manifold of the possible ground states due to frustration.

VII. EFFECTS OF MATERIALS STOCHASTICITY ON DEVICE AND SYSTEM MANUFACTURING PROCESSES

Advanced manufacturing processes by their very nature rely on process repeatability, i.e., limited in-process

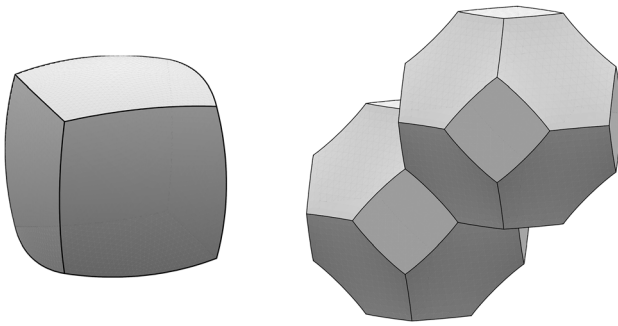


FIG. 18. Example of two polyhedral cells used to represent grains in an idealized material. The mean curvature of the cell faces is positive (left) and negative (right) under the constraint of a fixed external dihedral angle. Under normal grain growth conditions, these grains will shrink and grow respectively. For the assumed external dihedral angle, there is no constructible polyhedral cell having flat faces. The absence of constructible polyhedral cells with flat faces is an example of geometric frustration.

variations, to ensure the accuracy and the material properties of the final part/product manufactured. This becomes even more important while working with manufacturing processes at the micro and nano-scales where the inherent characteristics of scaled-down processes combined with a host of other factors such as variations in material micro/nanostructure and surface energy fluctuations make it extremely difficult to achieve process repeatability. A careful experimental investigation and subsequent modeling of the effects of stochasticity on micro/nano-scale manufacturing outcomes is needed

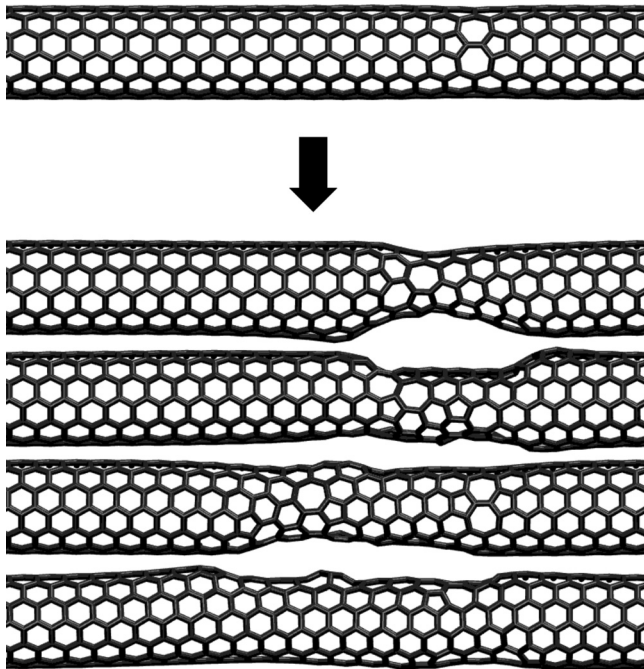


FIG. 19. Example of structural evolution of a carbon nanotube subjected to electron irradiation. The system is initially stretched by 8% to facilitate the creation of structural modifications. The figure at the top shows the initial system where a single Stone-Thrower-Wales (STW) or “5775” defect was created to partially release elongation strain energy. The system was then evolved at high temperature in four different computational runs using different seeds for the pseudo-random number generator used to choose the dynamical defect nucleation sites. Shown here are four resulting final structures, where stochasticity clearly leads to significantly different structures.

to ensure high process yields and desired property outcomes in the materials.

A field where stochastic variations are starting to influence, even limit, manufacturing is microelectronics. As the tolerances in device dimensions approach a few nm laterally, and the atomic scale vertically, fluctuations in inherent materials properties are posing substantial—even potentially insoluble—challenges. One pressing example is the variation in chain lengths in a polymer resist, used to define component dimensions within devices using optical lithography. The stochastic variation in end-to-end chain lengths—i.e., variations in the “tortuosity” of the polymer chains—is already a limiting factor in controlled linewidths,¹⁰¹ adding a few nm in edge roughness to average widths which are now approaching 10 nm or less. This can create intolerable variations in critical design parameters such as the gate length in the standard MOSFET (Metal-Oxide-Semiconductor Field Effect Transistor) device. Another upcoming “roadblock” is the variation in the number of dopant atoms that constitute a doped region of a device—such as the source, drain, or gate regions in a MOSFET. At ever decreasing device dimensions, the volumes of these different doped regions are becoming ever smaller, as are the number of dopant atoms contained within them. As these numbers reduce further, statistical fluctuations in these numbers will have an increasing effect on variations in local Fermi energies and hence upon device performance. Already a decade ago, a remarkable experiment has shown that controlled ion-by-ion introduction (using experimental methods that are ingenious but highly non-scalable to manufacturing) into device regions, as opposed to standard methods where a constant flux of ions is used to dope the material, produces substantially less variable device results (specifically, threshold voltages).¹⁰² These examples are illustrative of multiple such challenges in the microelectronics industries, where stochastic fluctuations in structure, chemistry, and properties create ever more challenging demands upon materials processing and manufacturing as device dimensions continue to shrink. This may even require new computing architectures to be evaluated and adopted (along with several other industry challenges such as power consumption and thermal management). This challenge is articulated beautifully in Poliakov *et al.*¹⁰³ where it is stated in the abstract “*The only way to keep pace with Moore’s Law is to use probabilistic computing for memory design. Probabilistic computing is ‘unavoidable,’ especially when scaled memory dimensions go down to the levels where variability takes over.*”

A. Detailed example—Additive manufacturing of hierarchical fiber-reinforced soft composites

As per the mathematical framework laid out in Sec. II, “forcing functions” represent interactions of the system with fields or perturbations that are not explicitly represented in the model. Manufacturing processes fall under the category of spatio-temporal forcing functions that influence the prediction of any QoI. These forcing functions comprise both deterministic as well as stochastic components. The deterministic

components originate from the repeatable/controllable aspects of the manufacturing process, whereas the stochastic components come from inherent fluctuations in the process variables that are outside the purview of closed-loop process control.¹⁰⁴ In this section, additive manufacturing of Hierarchical Fiber-reinforced Soft Composites (HFrSCs) is used as the detailed example to illustrate this concept. HFrSCs are an emerging class of materials consisting of polymeric fibers with specific material properties and hierarchical length-scales, embedded within another soft-polymer matrix.^{105,106} The applications of these soft composites include 4D printing, biomimetic composites, surgeon training, bioprinting, and embedded sensing/actuation.^{107–111} This example was specifically chosen because it builds on the mechanics of composites example presented in Sec. IV. Furthermore, the layer-by-layer technique used by additive manufacturing processes highlights how in some processes the spatio-temporal aspect of the “forcing function” becomes very critical in dictating the performance/properties of the final part. Here, we will first review the overall manufacturing process and its capabilities followed by a section highlighting the deterministic and stochastic components of the forcing function.

1. Process overview

The 3D printing process for HFrSCs was recently developed at Rensselaer Polytechnic Institute by Spackman *et al.*¹⁰⁵ Figure 20 outlines the process cycle developed to manufacture 3D multi-material, laminated HFrSC structures. The process first involves the manufacture of the roll of polymeric fibers using an electrospinning operation. Both aligned as well as randomly distributed fibers can be generated by appropriate design of the collector electrode. Once the fiber rolls have been manufactured, they are mounted on to a custom designed inkjet-based additive manufacturing setup (to print the 3D part).

The sequential processing steps involved in the manufacture of the laminated HFrSCs are as follows (Fig. 20):

- Step 1: Prepare a roll of fibers (aligned or randomly oriented) to be used during the 3D printing process;
- Step 2: Use the inkjet nozzles to print a layer of UV-curable polymer ink;
- Step 3: Expose the printed layer of polymer ink to UV light;
- Step 4: Dry the cured polymer surface using a heat lamp (optional);
- Step 5: Use a numerically programmed cutter to cut a section of the roll of fibers to the desired geometry of the layer;
- Step 6: Stamp the section of fibers on the dry polymer surface; and finally
- Step 7: Repeat Steps 2–6 for each layer as needed.

The integration of conventional inkjet-based 3D printing technology with an electrospinning-based fiber generation process not only makes it feasible to manufacture 3D laminated HFrSC structures but it also opens up a new frontier in soft-composite design. The above manufacturing process cycle can be easily adapted to print multiple polymeric inks and fibers into the same laminated structure to achieve hitherto unattainable material properties in the laminates.

In addition, the manufacturing process allows for a relatively straight forward scale-up to print macro-scale laminates containing nanofibers. This can be done by repeating the stamping operation over a larger area. The fiber loading in the laminate can also be easily varied by varying the frequency of the stamping operation [Figs. 20(b) and 20(c)]. For a given number-density of fibers in a roll, the highest loading of the fibers in the laminate can be obtained by stamping the fibers after depositing each single polymer layer, as seen in Fig. 20(b). This loading of fibers in the laminate can be reduced by reducing the frequency of the intermittent stamping operation as shown by the cross section of

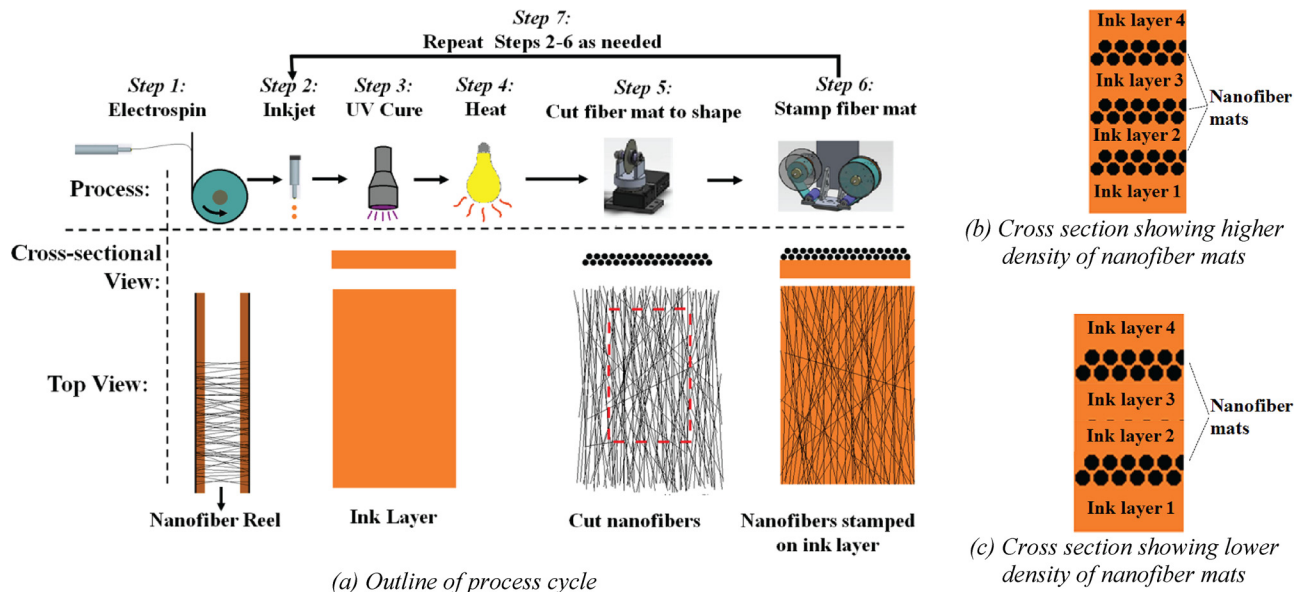


FIG. 20. Manufacturing process cycle for fabricating laminated hierarchical fiber-reinforced soft composite structures. (a) Outline of process cycle. (b) Cross section showing higher density of nanofiber mats. (c) Cross section showing lower density of nanofiber mats. Reproduced with permission from Spackman *et al.*, ASME J. Micro Nano Manuf. 3, 011008 (2015). Copyright 2015 American Society of Mechanical Engineers.

the sample in Fig. 20(c). The details related to the design of the electrospinning collectors and the 3D printer design can be found in Ref. 105. Figures 21(a)–21(c) show examples of a 3D printed structure manufactured using this process. Figure 21(d) depicts the cross section of the aligned composite laminate.

2. Implications on the forcing function

For the process outlined above, each of the key stages of manufacturing has associated deterministic and stochastic components that would influence the forcing function.

Process 1: Electrospinning—While the key process variables such as temperature/humidity conditions, solution concentration/flow-rates, electrode gaps, and voltages can be controlled during the fiber generation process, the following two uncontrolled variations exist in the system.

- (a) **Variation in the spacing density and alignment of fibers.** The electrospinning process inherently relies on the whipping instability of the liquid jet to generate the nanofibers. While the intelligent design of the collector results in collection of fiber mats, their local alignment and distribution cannot be well-controlled. This is highlighted particularly in Figs. 22(a) and 22(b), where one observes the formation of fiber clusters and voids in spite of the use of precision motion stages that can direct the deposition.
- (b) **Variation in properties of the fibers.** The properties of the fibers are a function of the polymer solutions used for the electrospinning process. In the case of multi-phase solutions, the quality of dispersion and the effects of the electric field on the agglomerates in the solution will affect the properties of the fibers. This is also true for core and shell-type fibers that involve multiple polymer solutions coming together to form the fiber.

Process 2: Inkjet printing process—This process uses a sequence of electric pulses to produce droplets in the 100 s of microns diameter range. For a given UV curable polymer ink, maintaining controlled temperature/humidity conditions will result in predictable droplet volumes. However, given that inkjet printing is conducted in open loop control, for the case of HrFScs, the following uncontrolled variation exists:

- (a) **Satellite droplets.** Occasional fluctuations in the system can result in satellite droplets that change the volume of liquid deposited.
- (b) **Droplet spreading.** While motion stages are precise, the spacing density and alignment variation seen in the fibers [refer to point (a) above for electrospinning] will affect the spreading pattern of the liquid. The graph in Figs. 22(a) and 22(b) shows the different spreading patterns seen when the droplet encounters the occasional fiber bundles or void spaces resulting from the non-uniform fibers deposited during the printing process. Figure 22(a) depicts a droplet landing between two fiber bundles and Fig. 22(b) depicts the case when voids are encountered in the fiber mat. The drastically different spreading times and patterns seen in the figures will affect the morphology of the layer being built, which in turn will affect the subsequent layers that follow. This phenomenon is also likely to induce variation in the extent of interpenetration between the fibers and the matrix. Given the layer-by-layer build pattern of the process, these variations are expected to have a cumulative effect on the overall property of the laminated composite.
- (c) **UV curing:** For most part, its influence can be assumed to be deterministic.

It is worth noting here that some of the layer-to-layer variations can be minimized by altering the printing protocols based on in-situ measurements. However, the error induced by the measurements will have to be considered as part of the forcing function. A good example of this is the

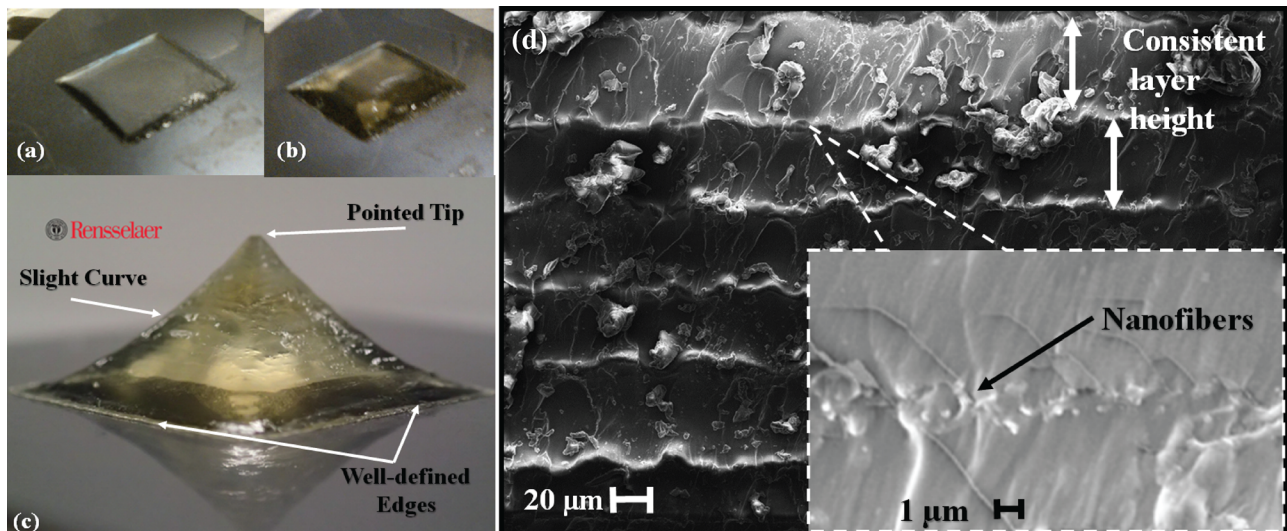


FIG. 21. 3D printed laminated composite (a) after 2 h, (b) after 9 h, and (c) final part after 17.5 h. (d) Cross-section. Reproduced with permission from Spackman *et al.*, ASME J. Micro Nano Manuf. 3, 011008 (2015). Copyright 2015 American Society of Mechanical Engineers.

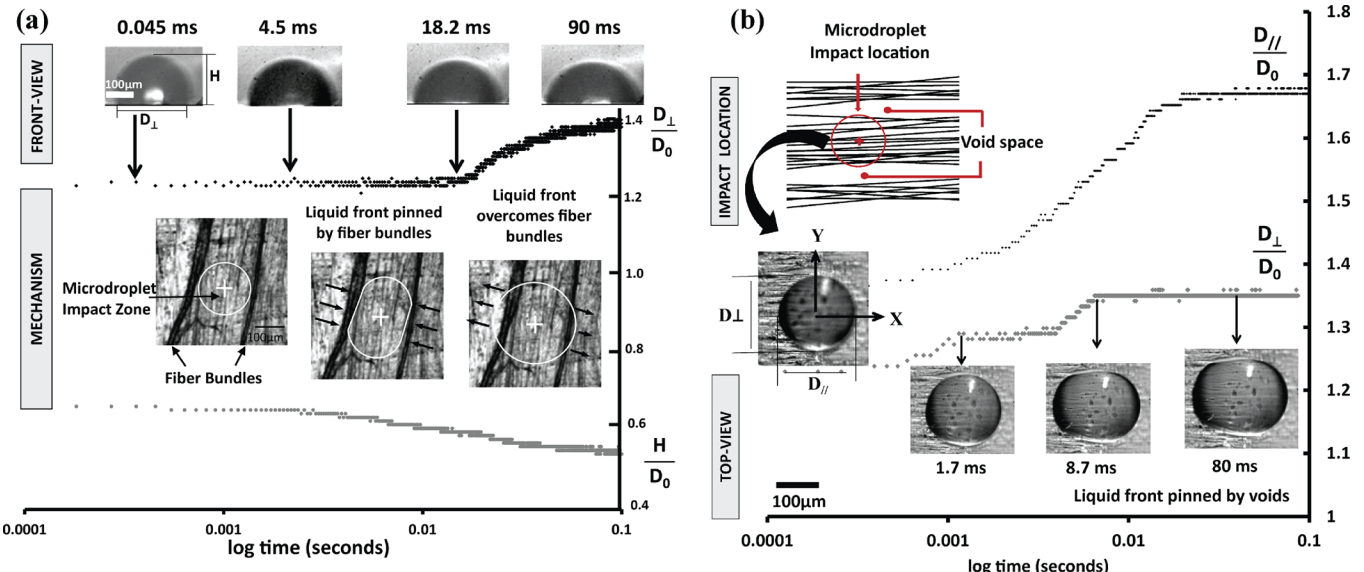


FIG. 22. Stochastic effects seen in droplet spreading. (a) Effect of fiber bundles in low-density mats seen in front-view. Here, the ratios (D_{\perp}/D_0) and (H/D_0) are indicated as a function of logarithmic timescale, where D_0 is the diameter of the droplet ejected by the inkjet nozzle, D_{\perp} is the diameter of the deposited droplet measured perpendicular to the direction of the alignment of the fibers, and H is the height of the droplet. The location of the droplet landing with respect to the fiber bundles is also shown. (b) Effect of voids in high-density mats seen in top-view. Here, the ratios (D_{\parallel}/D_0) and (D_{\perp}/D_0) are indicated as a function of logarithmic timescale, where D_{\parallel} is the diameter of the deposited droplet measured along the direction parallel to the alignment of the fibers. Reproduced with permission from Addit. Manuf. **12A**, 121 (2016). Copyright 2016 Elsevier.

metal additive manufacturing processes such as selective laser melting where while the temperature of the melt pool is monitored using a calibrated temperature sensor.¹¹² This sensor output is only an estimate of the temperature in the melt area and cannot be used as an absolute temperature to predict the evolution of the local microstructure. Therefore, error estimates need to be developed for the temperature measurement.

Process 3: Fiber stamping—In the HFrSC printing process, the fibers get transferred from the carrier substrate to the layer being printed. The following critical variation needs to be tracked in this particular case:

- (a) **Variation in number density of fibers transferred to the composite.** The manufacturing process relies on a mechanical stamping procedure to transfer the nano-fiber mats into the laminated structure. Even if the stamping load is controlled, this process has been observed to result in variable amounts of fibers being transferred to the composite. This is a function of the stochastic interactions between the fiber mats (which themselves have variations in their distribution) and the surface energy of the polymer surface that it is being stamped on to.

Manufacturing process variations have implications on the forcing function, which in turn affects the prediction and optimization problems described in Sec. II. For the prediction problem, the key will be to predict the QoI taking into consideration the uncertainties in the manufacturing forcing function. For the optimization problem, this would mean how can stochastic optimization specify an optimized ply structure (fiber size, spacing, number-density, etc.) for specific distribution of the QoI of interest in the presence of manufacturing uncertainties.

VIII. SUMMARY AND CONCLUSIONS

In this manuscript, we have sought to establish a framework for describing stochastic variations in material systems and to review how this concept is relevant—even in some cases dominant—to structure–property relationships.

Stochasticity can be inherent, or it can be engineered. An example of the former is the structure of multi-component glasses and of the latter is the dispersion of inclusions in a matrix to create a nanocomposite material. The resultant variations in structure and chemistry can occur over multiple length scales. The distribution function of atoms in a “random” crystalline or glass alloy will have components down to the atomic scale. Density fluctuations in a glass that are responsible for residual scattering in optical fibers typically occur over length scales of order a few nm. Variations in microstructure, often traceable to temporal fluctuations in nucleation phenomena, may occur over length scales up to 100 μm or even greater. The effects of these variations upon properties depend upon the length scale over which a property is established and how that matches to the length scale of the relevant structural/compositional fluctuation. Thus, electronic band structure is sensitive to fluctuations at atomic length scales. Electronic transport is most sensitive to fluctuations at length scales comparable to or greater than the carrier De Broglie wavelength (~10 nm). However, the relationship between length scale of fluctuation and length scale of the associated material property is often less immediate. For example, as stated above, the transmissivity of a state-of-the-art optical fiber is primarily limited by optical scattering from fluctuations at length scales much less (~nm) than the photon wavelength (~μm), due to Rayleigh scattering arising from the electronic polarizability of the constituent atoms of the glass. Nevertheless, the concept of understanding the length scales over which properties are

affected by fluctuations is critical to understanding the relationship between materials stochasticity and materials properties.

Control of stochasticity can thus lead to the fascinating possibility of an additional degree of freedom in creating new properties of materials or new performance of materials systems. While differences in properties between ordered and “random” (poly)crystalline alloys have been established for multiple materials systems, the property space for intermediate configurations of atomic order and fluctuation lengths scales have been hardly explored [Fig. 23]. However, the experimental and computational tools are emerging to explore these regimes. Extended X-Ray Absorption Fine Structure (EXAFS) is an established technique for determining atomic distribution functions in alloys and glasses.¹¹³ Atom probe tomography has emerged as an established method for measuring 3D atom-by-atom correlations in materials, although measurement of distribution functions in random or partly ordered materials are hindered by the difficulty in recording the full set of atoms in the structure.¹¹⁴ As discussed in Sec. III, Fluctuation Electron Microscopy (FM) and Small Angle X-Ray Scattering (SAXS) can interrogate fluctuations over intermediate length scales of nm to tens of nm. At larger length scales, for example, where microstructural variations due to stochasticity in nucleation and other kinetic phenomena dominate, a host of imaging and diffraction techniques with the necessary spatial resolution and chemical sensitivity exist. More challenging is the measurement of associated properties over the full range of length scales. The advent of scanning probe microscopy has enabled a broad range of surface properties to be measured with substantially higher spatial resolution, \sim 10 nm.¹¹⁵ Nano-indentation has also cast new light on mechanical properties at these length scales.¹¹⁶ However, many of these measurement techniques are known to perturb the property they are measuring and to be unable to access the interior rather than surface properties of a sample. Techniques for measurements at even shorter length scales, where many stochastic variations exist, are often indirect or non-existent. This is an area where considerable advances can be expected in the next decade, as new characterization techniques are constantly invented and developed, and the resolution limits

of photon, electron, and ion based methods continuously improve. Similarly, these questions will be increasingly addressed by highly accurate theoretical means, especially given the opportunities opened by the advent of larger and larger supercomputers which enable the explicit treatment of thousands of atoms, thereby providing a more realistic description of stochasticity at increasingly large length scales.

In this manuscript, we have organized stochasticity into four broad classes of materials origins: (1) Equilibrium fluctuations, arising from equilibrium concentrations of defects relative to a uniform structure (e.g., point defects in a crystal), (2) compositional or structural fluctuations, e.g., compositional or density fluctuations in a glass or partial order of a crystalline alloy, (3) kinetic fluctuations arising from transitions that are stochastic in time, such as nucleation phenomena, (4) frustration/degeneracy, arising from multiple equivalent equilibrium ground states, across which a system can stochastically distribute its components. In this review, we have focused on these stochasticity classes that relate directly to the material itself, but for completeness acknowledge two additional major sources of stochasticity that are not inherent to the material, (5) measurement stochasticity, where multiple non-equivalent states can appear equivalent—or non-equivalent states can be confused for each other—because of limited resolution or sensitivity of experimental measurements, (6) computational stochasticity, where inaccuracies or simplifications in computation and underlying physical models can confuse equivalent states of a system, or attribute multiple states to single state.

We further have classified materials (1–4 above) stochastic origins as *inherent* or *engineered*, depending on whether they occur without external intervention (inherent), or are designed through external intervention (engineered). Of course, even inherent stochasticities can be influenced or controlled through control of state variables such as temperature and pressure. This suggests again that a rich new property parameter space can be realized through exploration of the internal region of Fig. 23.

We have illustrated the results of these stochastic origins upon materials properties and performance using as case studies density fluctuations and medium range order in

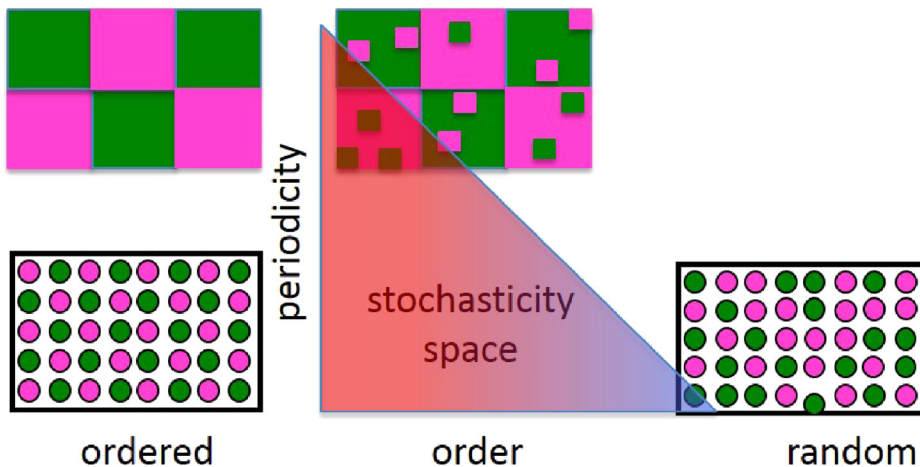


FIG. 23. Illustration of stochasticity space in alloy materials, demonstrating the ability to explore combinations of atomic-level compositional disorder and periodic modulations to tailor material properties.

glasses; the effects of filler distributions upon mechanical properties of artificial and natural (bone) nanocomposites; nucleation phenomena including phase transformations, deformation twinning, and fatigue cracking; degenerate ground states in defective carbon nanotubes; and materials processing during additive manufacturing. Beyond these examples, it is our thesis that stochastic processes influence properties and/or performance, in principle, in all materials systems, and in practice play a significant role in most. Thus, a comprehensive understanding and control of materials stochasticity offers a major opportunity for both improving materials performance and discovering new parameter space in the coming decades. Finally, we believe that this concept is a critical—and currently largely unrecognized—dimension of realizing the goals of the Materials Genome Initiative.

ACKNOWLEDGMENTS

We acknowledge the following funding support for parts of the work described in this review:

NSF CMMI 1462648 (J.S.), NSF CMMI 1334283 (R.H., D.L., and A.M.), NSF CMMI 1363526 (D.V. and C.P.), NSF DMR 1056704 (D.L.), NSF DMR 1265100 (M.T.), NYSTAR C13017 and C15017 (R.H., P.K., and V.M.), and internal funding from the RPI Office of the Vice-President for Research.

¹See, for example, J. P. Bentley, “The accuracy of measurement systems in the steady state,” in *Principles of Measurement Systems* (Longman Scientific, Singapore, 1995), Chap. 3.

²See, for example, D. Hoffman and F. Ernst, *Ultramicroscopy* **53**, 205 (1994).

³See, for example, S. V. Kalinin, E. Strelcov, A. Belianinov, S. Somnath, R. K. Vasudevan, E. J. Lingerfelt, R. K. Archibald, C. Chen, R. Proksch, N. Laanait, and S. Jesse, *ACS Nano* **10**, 9068 (2016).

⁴J. M. Murphy, D. M. Sexton, D. N. Barnett, G. S. Jones, M. J. Webb, M. Collins, and D. A. Stainforth, *Nature* **430**, 768 (2004).

⁵M. Anisworth and J. T. Oden, *A Posteriori Error Estimation in Finite Element Analysis* (John Wiley, 2000).

⁶R. C. Picu, Z. Li, M. A. Soare, S. Sorohan, D. M. Constantinescu, and E. Nutu, *Mech. Mater.* **69**, 251 (2014).

⁷H. Mori, *Prog. Theor. Phys.* **33**, 423 (1965).

⁸R. Zwanzig, *J. Stat. Phys.* **9**, 215 (1973).

⁹W. L. Oberkampf, T. G. Trucano, and C. Hirsch, *Appl. Mech. Rev.* **57**, 345–384 (2004).

¹⁰H. Niederreiter, “Random Number Generation and Quasi-Monte Carlo Methods,” *CBMS-NSF Regional Conference Series in Applied Mathematics* (Society for Industrial and Applied Mathematics, Philadelphia, 1992).

¹¹“Monte Carlo and quasi-Monte Carlo methods,” in Proceeding of the Second International Conference on Monte Carlo and quasi-Monte Carlo Methods in Scientific Computing, edited by H. Niederreiter *et al.* (Springer-Verlag, New York, 1998), Vol. 127.

¹²E. Novak and K. Ritter, *Constr. Approx.* **15**, 499 (1999).

¹³D. Xiu, *Commun. Comput. Phys.* **5**, 242 (2009).

¹⁴R. G. Ghanem and P. D. Spanos, *Stochastic Finite Elements: A Spectral Approach* (Dover Publications, Mineola, NY, 2012).

¹⁵I. Babuska, R. Tempone, and G. E. Zouraris, *SIAM J. Numer. Anal.* **42**, 800 (2004).

¹⁶J. Mohan, O. Sahni, A. Doostan, and A. A. Oberai, *SIAM/ASA J. Uncertainty Quantification* **2**, 397 (2014).

¹⁷D. Xiu, *Commun. Comput. Phys.* **2**, 293 (2007).

¹⁸A. Doostan and H. Owhadi, *J. Comput. Phys.* **230**, 3015 (2011).

¹⁹H. Robbins and S. Monro, *Ann. Math. Stat.* **22**, 400 (1951).

²⁰L. Bottou, “Large-scale machine learning with stochastic gradient descent,” in *Proceeding of COMPSTAT* (Physica-Verlag, Heidelberg, 2010), pp. 177–186.

²¹G. Calafiore and M. C. Campi, *Math. Programming* **102**, 25 (2005).

²²M. Bayes and M. Price, *Philos. Trans.* **53**, 370 (1763).

²³J. P. Huelsenbeck and F. Ronquist, *Bioinformatics* **17**, 754 (2001).

²⁴G. E. Box and G. C. Tiao, *Bayesian Inference in Statistical Analysis* (John Wiley & Sons, NY, 1992).

²⁵Y. M. Marzouk, H. N. Najm, and L. A. Rahn, *J. Comput. Phys.* **224**, 560 (2007).

²⁶A. Q. Tool, *J. Am. Ceram. Soc.* **29**, 240 (1946).

²⁷C. Levelut, A. Faivre, R. L. Parc, B. Champagnon, J.-L. Hazemann, L. David, C. Rochas, and J.-P. Simon, *J. Non-Cryst. Solids* **307-310**, 426 (2002).

²⁸L. D. Landau and E. M. Lifshitz, *Statistical Physics*, 2nd ed. (Addison-Wesley, Reading, MA, 1969).

²⁹C. J. Montrose, V. A. Solovev, and T. A. Litovitz, *J. Am. Soc. Acoust.* **43**, 117 (1968).

³⁰D. A. Pinnow, S. J. Candau, J. T. LaMacchia, and T. A. Litovitz, *J. Am. Soc. Acoust.* **43**, 131 (1968).

³¹N. L. laberge, V. V. Basilescu, C. J. Montrose, and P. B. Macdo, *J. Am. Ceram. Soc.* **56**, 506 (1973).

³²J. Zarzycki, *Glasses and the Vitreous State*, translated by W. D. Scott and C. Massart (Cambridge University Press, Cambridge, England, 1982).

³³J. H. Konnert, J. Karle, and G. A. Ferguson, *Science* **179**, 177 (1973).

³⁴T. Watanabe, K. Saito, and J. Ikushima, *J. Appl. Phys.* **94**, 4824 (2003).

³⁵T. Watanabe, K. Saito, and A. J. Ikushima, *J. Appl. Phys.* **95**, 2432 (2004).

³⁶H. Kakiuchida, E. H. Sekiya, K. Saito, and A. J. Ikushima, *Jpn. J. Appl. Phys., Part 2* **42**, L1526 (2003).

³⁷A. B. Bhatia and D. E. Thornton, *Phys. Rev. B* **2**, 3004 (1970).

³⁸J. H. Simmons, A. Napolitano, and P. B. Macedo, *J. Chem. Phys.* **53**, 1165 (1970).

³⁹M. Tomozawa, “Phase separation in glass,” in *Treatise on Materials Science and Technology: Glass II*, edited by M. Tomozawa and R. H. Doremus (Academic Press, New York, 1979), p. 71.

⁴⁰V. McGahay and M. Tomozawa, *J. Non-Cryst. Solids* **109**, 27 (1989).

⁴¹S. Fujita, Y. Kato, and M. Tomozawa, *J. Non-Cryst. Solids* **328**, 64 (2003).

⁴²H. N. Ritland, *J. Am. Ceram. Soc.* **39**, 403 (1956).

⁴³A. J. Kovacs, *Fortschr. Hochpoly-Forsch. (Adv. Polym. Sci.)* **3**, 394 (1963).

⁴⁴D. P. B. Aji, P. Wen, and G. P. Johari, *J. Non-Cryst. Solids* **353**, 3796 (2007).

⁴⁵P. B. Macedo and A. Napolitano, *J. Res. Natl. Bur. Standards* **71A**, 231 (1967).

⁴⁶A. Koike, S. R. Ryu, and M. Tomozawa, *J. Non-Cryst. Solids* **351**, 3797 (2005).

⁴⁷A. C. Hannon, D. I. Grimly, R. A. Hulme, A. C. Wright, and R. N. Sinclair, *J. Non-Cryst. Solids* **177**, 299 (1994).

⁴⁸D. L. Kim and M. Tomozawa, *J. Non-Cryst. Solids* **286**, 132 (2001).

⁴⁹D. L. Kim, M. Tomozawa, S. Dubios, and G. Orcel, *J. Lightwave Technol.* **19**, 1155 (2001).

⁵⁰K. Saito, M. Yamaguchi, H. Kakiuchida, and A. J. Ikushima, *Appl. Phys. Lett.* **83**, 5175 (2003).

⁵¹C. Zener, *Elasticity and Anelasticity of Metals* (University of Chicago Press, Chicago, 1948), p. 100.

⁵²A. Guinier and G. Fournet, *Small Angle Scattering of X-Rays* (John Wiley & Sons, NY, 1955) (Translated by Christopher B. Walker, followed by a bibliography by Kenneth L. Yudowitch).

⁵³H. Z. Cummins and R. W. Gammon, *J. Chem. Phys.* **44**, 2785 (1966).

⁵⁴J. Schroeder, “Light scattering of glass,” in *Treatise on Materials Science and Technology: Glass I*, edited by M. Tomozawa and R. H. Doremus (Academic Press, NY, 1977), Vol. 12, p. 157.

⁵⁵P. Lamparter and S. Steeb, *J. Non-Cryst. Solids* **106**, 137 (1988).

⁵⁶M. M. J. Treacy and J. M. Gibson, *Acta Crystallogr. A* **52**, 212 (1996).

⁵⁷L. Fan, I. McNulty, D. Paterson, M. M. J. Treacy, and J. M. Gibson, *Neutron and X-Ray Scattering as Probes of Multiscale Phenomena*, edited by S. R. Bhatia *et al.* (Materials Research Society, Warrendale, 2005), Vol. 840, pp. Q6.7.1–Q6.7.6.

⁵⁸J. M. Gibson and M. M. J. Treacy, *Phys. Rev. Lett.* **78**, 1074 (1997).

⁵⁹F. Wooten, K. Winer, and D. Weaire, *Phys. Rev. Lett.* **54**, 1392 (1985).

⁶⁰K. Ding and H. C. Andersen, *Phys. Rev. B* **10**, 6987 (1986).

⁶¹P. C. Kelires and J. Tersoff, *Phys. Rev. Lett.* **61**, 562 (1988).

⁶²W. D. Luedtke and U. Landman, *Phys. Rev. B* **40**, 1164 (1989).

⁶³M. M. J. Treacy, J. M. Gibson, and P. J. Kebinski, *J. Non-Cryst. Solids* **231**, 99 (1998).

⁶⁴J. Li, X. Gu, and T. C. Hufnagel, *Microsc. Microanal.* **9**, 509 (2003).

⁶⁵L. He, J. P. Chu, C.-L. Li, C.-M. Lee, Y.-C. Chen, P. K. Liaw, and P. M. Voyles, *Thin Film Solids* **561**, 87 (2014).

- ⁶⁶P. M. Voyles, Ph.D. dissertation (University of Illinois at Urbana-Champaign, Department of Physics, 2001).
- ⁶⁷P. Hirsch, A. Howie, R. Nicholson, W. Pashley, and M. J. Whelan, *Electron Microscopy of Thin Crystals* (Krieger Publishing Co, Malabar, FL, 1977), p. 156.
- ⁶⁸R. K. Dash, P. Voyles, M. Gibson, M. M. Treacy, and P. Keblinski, *J. Phys. Condens. Matter* **15**, S2425 (2003).
- ⁶⁹S. Torquato, *Random Heterogeneous Materials: Microstructure and Macroscopic Properties* (Springer, New York, 2002).
- ⁷⁰G. J. Dvorak, *Mechanics of Composite Materials* (Springer, New York, 2013).
- ⁷¹S. Nemat-Nasser and M. Hori, *Micromechanics: Overall Properties of Heterogeneous Materials* (North-Holland, Amsterdam, 1999).
- ⁷²R. C. Picu, S. Sorohan, M. A. Soare, and D. M. Constantinescu, *Mech. Mater.* **97**, 59 (2016).
- ⁷³E. Ban, V. H. Barocas, M. S. Shephard, and R. C. Picu, *J. Mech. Phys. Solids* **87**, 38 (2016).
- ⁷⁴S. D. Dimas, D. Veneziano, T. Giesa, and M. J. Buehler, *J. Appl. Mech.* **82**, 011003 (2015).
- ⁷⁵S. Kanuparthi, G. Subbarayan, T. Siegmund, and B. Sammakia, *IEEE Trans. Compon. Packaging Technol.* **32**, 424 (2009).
- ⁷⁶V. Negi and R. C. Picu, “Elastic-plastic transition in stochastic heterogeneous materials: size effect and triaxiality,” *Mech. Mater.* (in press).
- ⁷⁷A. A. Poundarik, T. Diab, G. E. Sroga, A. Ural, A. L. Boskey, C. M. Gundberg, and D. Vashishth, *Proc. Nat. Acad. Sci. U.S.A.* **109**, 19178 (2012).
- ⁷⁸J. W. Christian and S. Mahajan, “Deformation twinning,” *Prog. Mater. Sci.* **39**, 1 (1995).
- ⁷⁹J. Wang, S. K. Yadav, J. P. Hirth, C. N. Tomé, and I. J. Beyerlein, *Mater. Res. Lett.* **1**, 126 (2013).
- ⁸⁰I. J. Beyerlein, L. Capolungo, P. E. Marshall, R. J. McCabe, and C. N. Tomé, *Philos. Mag.* **90**, 2161 (2010).
- ⁸¹S. R. Niezgoda, A. K. Kanjaria, I. J. Beyerlein, and C. N. Tomé, *Int. J. Plast.* **56**, 119 (2014).
- ⁸²I. J. Beyerlein and C. N. Tomé, *Proc. R. Soc. London, Ser. A* **466**, 2517 (2010).
- ⁸³Y. Liu, M. Weinert, and L. Li, *Phys. Rev. Lett.* **108**, 115501 (2012).
- ⁸⁴A. V. Latyshev, A. L. Aseev, A. B. Krasilnikov, and S. I. Stenin, *Surf. Sci.* **213**, 157 (1989).
- ⁸⁵J. Gómez-Gardeñes and V. Latora, *Phys. Rev. E* **78**, 065102(R) (2008).
- ⁸⁶S. B. Zhang and J. E. Northrup, *Phys. Rev. Lett.* **67**, 2339 (1991).
- ⁸⁷P. Hohenberg and W. Kohn, *Phys. Rev. B* **136**, B864 (1964).
- ⁸⁸W. Kohn and L. J. Sham, *Phys. Rev.* **140**, A1133 (1965).
- ⁸⁹F. J. Humphreys and M. Hatherly, *Recrystallization and Related Annealing Phenomena*, 2nd ed. (Elsevier, New York, 2004), pp. 250–260.
- ⁹⁰R. D. Doherty, *Met. Sci. J.* **8**, 132 (1974).
- ⁹¹M. G. Ardakani and F. J. Humphreys, *Acta Metall.* **42**, 763 (1994).
- ⁹²R. D. Doherty and J. A. Szpunar, *Acta Metall.* **32**, 1789 (1984).
- ⁹³L. Christodoulou and J. Larsen, *JOM* **56**, 15 (2004).
- ⁹⁴J. E. Bozek, J. D. Hochhalter, M. G. Vielleux, M. Liu, G. Heber, S. D. Sintay, A. D. Rollett, D. J. Littlewood, A. M. Maniatty, H. Weiland, R. J. Christ, Jr., J. Payne, G. Welsh, D. G. Harlowe, P. A. Wawrzynek, and A. R. Ingraffea, *Modell. Simul. Mater. Sci. Eng.* **16**, 065007 (2008).
- ⁹⁵J. D. Hochhalter, D. J. Littlewood, R. J. Christ, Jr., M. G. Vielleux, J. E. Bozek, A. R. Ingraffea, and A. M. Maniatty, *Modell. Simul. Mater. Sci. Eng.* **18**, 045004 (2010).
- ⁹⁶J. D. Hochhalter, D. J. Littlewood, M. G. Vielleux, J. E. Bozek, A. M. Maniatty, A. D. Rollett, and A. R. Ingraffea, *Modell. Simul. Mater. Sci. Eng.* **19**, 035008 (2011).
- ⁹⁷P. Paris and F. Erdogan, *ASME Trans., J. Basic Eng.* **85**, 528 (1963).
- ⁹⁸O. T. Benfey, *J. Chem. Educ.* **35**, 21 (1958).
- ⁹⁹M. E. Glicksman, P. R. Rios, and D. J. Lewis, *Int. J. Mater. Res.* **100**, 536 (2009).
- ¹⁰⁰A. V. Krasheninnikov and F. Banhart, *Nat. Mater.* **6**, 723 (2007).
- ¹⁰¹See, for example, J. Y. Cheng, C. T. Rettner, D. P. Sanders, H.-C. Kim, and W. D. Hinsberg, *Adv. Mater.* **20**, 3155 (2008).
- ¹⁰²T. Shinada, S. Okamoto, T. Kobayashi, and I. Ohdomari, *Nature* **437**, 1128 (2005).
- ¹⁰³P. Poliakov, P. Blomme, A. V. Pret, M. M. Corbalan, R. Gronheid, D. Verkest, J. Van Houdt, and W. Dehaene, *Microelectron. Reliab.* **52**, 525 (2012).
- ¹⁰⁴D. Djurdjanovic, L. Mears, F. A. Niaki, A. U. Haq, and L. Li, in *Proceedings of the 12th ASME International Manufacturing Science and Engineering Conference (MSEC)* (2017), Vol. 1, p. 3104.
- ¹⁰⁵C. Spackman, K. Picha, G. Gross, J. Nowak, P. J. Smith, J. Zheng, J. Samuel, and S. Mishra, *ASME J. Micro Nano Manuf.* **3**, 011008 (2015).
- ¹⁰⁶K. Picha, C. Spackman, and J. Samuel, *Addit. Manuf.* **12A**, 121 (2016).
- ¹⁰⁷S. Tibbits, *Archit. Des.* **84**, 116 (2014).
- ¹⁰⁸Q. Ge, J. J. Qi, and M. L. Dunn, *Appl. Phys. Lett.* **103**, 131901 (2013).
- ¹⁰⁹S. Lapidot, S. Meirovitch, S. Sharon, A. Heyman, D. L. Kaplan, and O. Shoseyov, *Nanomedicine* **7**, 1409 (2012).
- ¹¹⁰F. Yan, Y. Liu, H. Chen, F. Zhang, L. Zheng, and Q. Hu, *AIP Adv.* **4**, 031321 (2014).
- ¹¹¹J. Czyzewski, P. Burzynski, K. Gawe, and J. Meisner, *J. Mater. Process. Technol.* **209**, 5281 (2009).
- ¹¹²S. K. Everton, M. Hirsch, P. Stravroulakis, R. K. Leach, and A. T. Clare, *Mater. Des.* **95**, 431 (2016).
- ¹¹³See, for example, V. L. Aksenov, M. V. Koval’chuk, A. Y. Kuz’mín, Yu. Purans, and S. I. Tyutyunnikov, *Crystallogr. Rep.* **51**, 908 (2006).
- ¹¹⁴See, for example, T. F. Kelly and M. K. Miller, *Rev. Sci. Instrum.* **78**, 31101 (2007).
- ¹¹⁵See, for example, papers in “Nanoscale 13,” Foreword by L. Koenders and S. Ducourtieux, *Meas. Sci. Technol.* **25**(4), 040301 (2014).
- ¹¹⁶See, for example, O. C. Warren and G. M. Pharr, *MRS Bull.* **35**, 897 (2010).